The Company of **Biologists**

RESEARCH ARTICLE

Phospholipid composition and a polybasic motif determine D6 PROTEIN KINASE polar association with the plasma membrane and tropic responses

Inês C. R. Barbosa[1], Hiromasa Shikata[1], Melina Zourelidou[1], Mareike Heilmann[2], Ingo Heilmann[2] and Claus Schwechheimer[1,*]

ABSTRACT

Polar transport of the phytohormone auxin through PIN-FORMED (PIN) auxin efflux carriers is essential for the spatiotemporal control of plant development. The *Arabidopsis thaliana* serine/threonine kinase D6 PROTEIN KINASE (D6PK) is polarly localized at the plasma membrane of many cells where it colocalizes with PINs and activates PIN-mediated auxin efflux. Here, we show that the association of D6PK with the basal plasma membrane and PINs is dependent on the phospholipid composition of the plasma membrane as well as on the phosphatidylinositol phosphate 5-kinases PIP5K1 and PIP5K2 in epidermis cells of the primary root. We further show that D6PK directly binds polyacidic phospholipids through a polybasic lysine-rich motif in the middle domain of the kinase. The lysine-rich motif is required for proper PIN3 phosphorylation and for auxin transport-dependent tropic growth. Polybasic motifs are also present at a conserved position in other D6PK-related kinases and required for membrane and phospholipid binding. Thus, phospholipid-dependent recruitment to membranes through polybasic motifs might not only be required for D6PK-mediated auxin transport but also other processes regulated by these, as yet, functionally uncharacterized kinases.

KEY WORDS: D6PK, Auxin transport, Phospholipid, Lysine-rich motif, Plasma membrane

INTRODUCTION

The phytohormone auxin is essential for plant differentiation and growth (Leyser, 2010; Teale et al., 2006). Seemingly all organ development as well as all dynamic tropic growth responses, e.g. phototropism and gravitropism, rely on differential auxin distribution patterns and auxin-induced cellular responses (Adamowski and Friml, 2015; Wang and Estelle, 2014). Auxin levels within the plant are controlled by local auxin metabolism and directional auxin transport, which is achieved by the PIN-FORMED (PIN) efflux and the AUXIN RESISTANT 1/LIKE AUX1 (AUX1/ LAX) influx carriers (Adamowski and Friml, 2015). PINs are polarly distributed in the plasma membranes of many cells and their differential distribution results in the formation of local auxin maxima and minima that orchestrate the development of the

growing plant body (Adamowski and Friml, 2015; Grunewald and Friml, 2010; Habets and Offringa, 2014).

Studies on directional auxin transport and PIN polar distribution have become attractive systems to study cell polarity in plants (Pan et al., 2015; Sachs, 1991; Yang, 2008). Although it is still unclear whether the targeting of *de novo* synthesized PINs is polar or apolar, it is well established that the maintenance of PIN polarity requires constitutive recycling in combination with a reduced lateral diffusion in the plasma membrane (Feraru et al., 2011; Kleine-Vehn et al., 2011). PIN polarity is seemingly also critically dependent on the activity of the AGCVIII protein kinase PINOID (PID) and PIN phosphorylation (Friml et al., 2004; Kleine-Vehn et al., 2009; Michniewicz et al., 2007; Offringa and Huang, 2013). Tissue-specific PIN polar distribution patterns can sufficiently explain auxin distribution gradients across plant organs like roots and shoots (de Reuille et al., 2006; Grieneisen et al., 2007; Heisler et al., 2010; Mironova et al., 2010; van Berkel et al., 2013; Wabnik et al., 2011). Additionally, gravity as well as light-dependent changes in PIN polarity correlate with observed changes in auxin distribution required for tropic growth processes (Ding et al., 2011; Kleine-Vehn et al., 2010; Rakusová et al., 2011). Thus, understanding PIN polarity and activity control at the plasma membrane can substantially contribute to the understanding of plant growth.

PIN-mediated auxin transport is critically dependent on phosphorylation by protein kinases (Barbosa and Schwechheimer, 2014). The AGCVIII serine/threonine kinase D6 PROTEIN KINASE (D6PK) but also the proposed PIN polarity regulator PINOID (PID) activate PIN-mediated auxin transport through PIN phosphorylation when tested in *Xenopus laevis* oocytes (Friml et al., 2004; Zourelidou et al., 2014). *Arabidopsis* mutants of *D6PK* and the orthologous *D6PK-LIKE* genes *D6PKL1-D6PKL3* are compromised in directional auxin transport and PIN-dependent growth (Willige et al., 2013; Zourelidou et al., 2009). Conversely, pharmacological interference with D6PK abundance at the plasma membrane impairs auxin transport-dependent tropic responses (Barbosa et al., 2014). Although both D6PK and PINs are polarly localized at the plasma membranes of cells of different plant tissues, their recycling kinetics are dramatically different and obviously mediated by different trafficking pathways (Barbosa et al., 2014; Geldner et al., 2003; Zourelidou et al., 2009). Understanding how D6PK associates with the plasma membrane is thus important for understanding D6PK-mediated auxin transport and plant growth regulation.

Peripheral membrane proteins can be anchored to membranes by diverse mechanisms that include protein-protein and protein-lipid interactions (Cho and Stahelin, 2005). The very low abundant phosphoinositides (PIs) are important players for the recruitment of

[1]Plant Systems Biology, Technische Universität München, Emil-Ramann-Strasse 8, Freising 85354, Germany. [2]Institute for Biochemistry and Biotechnology, Cellular Biochemistry, Martin-Luther-Universität Halle-Wittenberg, Kurt-Mothes-Strasse 3, Halle 06120, Germany.

*Author for correspondence (claus.schwechheimer@wzw.tum.de)

I.H., 0000-0002-2324-1849; C.S., 0000-0003-0269-2330

DEVELOPMENT

peripheral proteins to membranes (Balla, 2013; Heilmann, 2016). PIs are mono-, bis- and tris-phosphorylated derivatives of phosphatidylinositol (PtdIns) and PI compositions differ between the plasma membrane and different organellar membranes (Balla, 2013). Membrane-specific PI distribution, a result of the differential distribution and tight regulation of specific PI kinases or phosphatases, allows recruiting specific cognate binding proteins that determine organelle function (Behnia and Munro, 2005). In particular, asymmetric PI distribution in the plasma membrane contributes to the organization of polar domains in many organisms and biological processes (Comer and Parent, 2007; McCaffrey and Macara, 2009; Orlando and Guo, 2009; Shewan et al., 2011). In plants, the polar distribution of PIs, PI kinases, PI binding partners and associated processes are extensively studied in tip growing cells such as pollen tubes and root hairs (Kusano et al., 2008; Stenzel et al., 2008; Ischebeck et al., 2010). Analysis of PtdIns$(4,5)$P$_2$ biosensors and respective PIP5Ks (PtdIns4P 5-KINASES) revealed that PtdIns$(4,5)$P$_2$ and PIP5Ks are polarly localized in many cell types and required for PIN polarity control (Ischebeck et al., 2013; Tejos et al., 2014). More recently, PtdIns4P was identified as a major PI, conferring negative charges to the plant plasma membrane (Simon et al., 2016).

Peripheral membrane proteins can bind PIs through globular PI species-specific binding domains, e.g. the PtdIns3P-specific FYVE domain or the PtdIns$(4,5)$P$_2$-specific PH domain (Hammond and Balla, 2015). Alternatively, peripheral membrane proteins can bind membranes through ionic interactions between stretches of positively charged basic amino acids [lysine (K) or arginine (R)] and the negatively charged lipids, such as PIs or PtdOH (phosphatidic acid) (Brzeska et al., 2010; Heo et al., 2006; Jaillais et al., 2011; McLaughlin and Murray, 2005).

D6PK associates also with root hair tips following root hair initiation (Stanislas et al., 2015). PINs, the established D6PK substrates, are reportedly absent from root hair tips and D6PK might have other phosphorylation substrates and PIN-independent roles at this plasma membrane region (Stanislas et al., 2015). The association of D6PK with the root hair initiation site is dependent on PIP5K3 and, reciprocally, D6PK can bind phospholipids *in vitro* (Stanislas et al., 2015). A basic sequence stretch noted in several AGCVIII kinases is a good candidate region for phospholipid interactions (Zegzouti et al., 2006).

Here, we show that D6PK is able to bind phospholipids with polyacidic headgroups and that phospholipid composition critically determines D6PK plasma membrane recruitment and polarity. We further identify a polybasic K-rich motif within the D6PK middle domain that is required for D6PK phospholipid binding and membrane association as well as for proper PIN phosphorylation and PIN-dependent tropisms. Additionally, we find that K/R-rich motifs are essential for membrane and phospholipid-binding in other, as yet, uncharacterized AGCVIII kinases. Thus, phospholipid-dependent recruitment of AGCVIII kinases through ionic interactions between the polyacidic phospholipid headgroups and polybasic motifs emerge as general control mechanisms of protein-membrane binding, and in the case of D6PK for auxin transport control.

RESULTS
D6PK plasma membrane association is phospholipid dependent

The molecular determinants of the membrane association and polar distribution of D6PK at the basal plasma membrane of root cells are unknown. In lipid overlay assays, D6PK bound to phospholipids with polyacidic headgroups, namely phosphatidic acid (PtdOH) as well as the PIs PtdIns3P, PtdIns4P, PtdIns5P, PtdIns$(3,4)$P$_2$, PtdIns$(3,5)$P$_2$, PtdIns$(4,5)$P$_2$ and PtdIns$(3,4,5)$P$_3$ (Fig. 1A). D6PK binding was strongest to PtdIns3P when using TRIS-buffered saline and to PtdOH when using PBS (phosphate-buffered saline) of comparable ionic strengths (188 mM and 181 mM) (Fig. 1A) (Stanislas et al., 2015). D6PK did not bind to phospholipids with neutral headgroups, namely PtdCho (phosphatidylcholine) and PtdEtn (phosphatidylethanolamine), or to phospholipids with monoacidic headgroups such as PtdIns and phosphatidylserine (PtdSer; Fig. 1A). In a lipid bilayer context using liposomes of mixed phospholipid compositions, D6PK bound to liposomes containing the polyacidic phospholipids PtdIns4P, PtdIns$(4,5)$P$_2$ or PtdOH, but not to liposomes containing only PtdEtn and PtdCho, phospholipids with neutral headgroups (Fig. 1B).

PI biosynthesis begins with PtdIns and involves several phosphorylation and dephosphorylation steps by PI kinases and phosphatases (Meijer and Munnik, 2003). PtdOH, conversely, is produced either from PIs by phosphoinositide phospholipase C (PI-PLC) and subsequent action of diacylglycerol kinase (DGK) or from PtdCho or PtdEtn by phospholipase D (PLD; Fig. 2A) (Meijer and Munnik, 2003). To address whether the membrane phospholipid composition determined the basal localization of
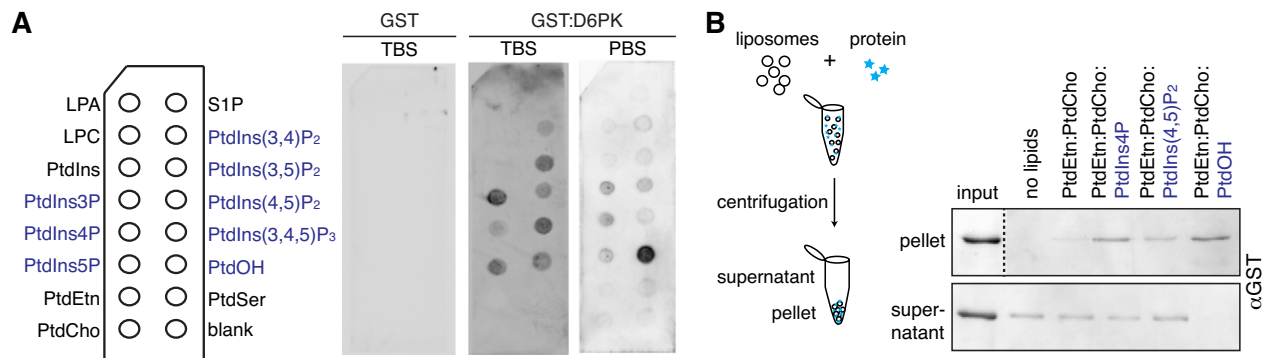
Fig. 1. D6PK binds to polyacidic phospholipids. (A) Lipid overlay assay with purified GST and GST:D6PK using TBS and PBS buffers. Abbreviations: LPA, lysophosphatidic acid; LPC, lysophosphatidylcholine; PtdIns, phosphatidylinositol and its mono-/bis-/tris-phosphates; PtdEtn, phosphatidyl-ethanolamine; PtdCho, phosphatidylcholine; S1P, sphingosine-1-phosphate; PtdOH, phosphatidic acid; PtdSer, phosphatidylserine. (B) Anti-GST immunoblot of GST:D6PK after liposome binding assays using lipid mixtures containing the neutral PtdEtn and neutral PtdCho mixed with either of the polyacidic PtdIns4P, PtdIns$(4,5)$P$_2$, or PtdOH as specified. The experiment was repeated twice, one representative blot is shown. All samples from the upper panel are from the same blot; the blot was spliced to eliminate the marker lane (dashed line).
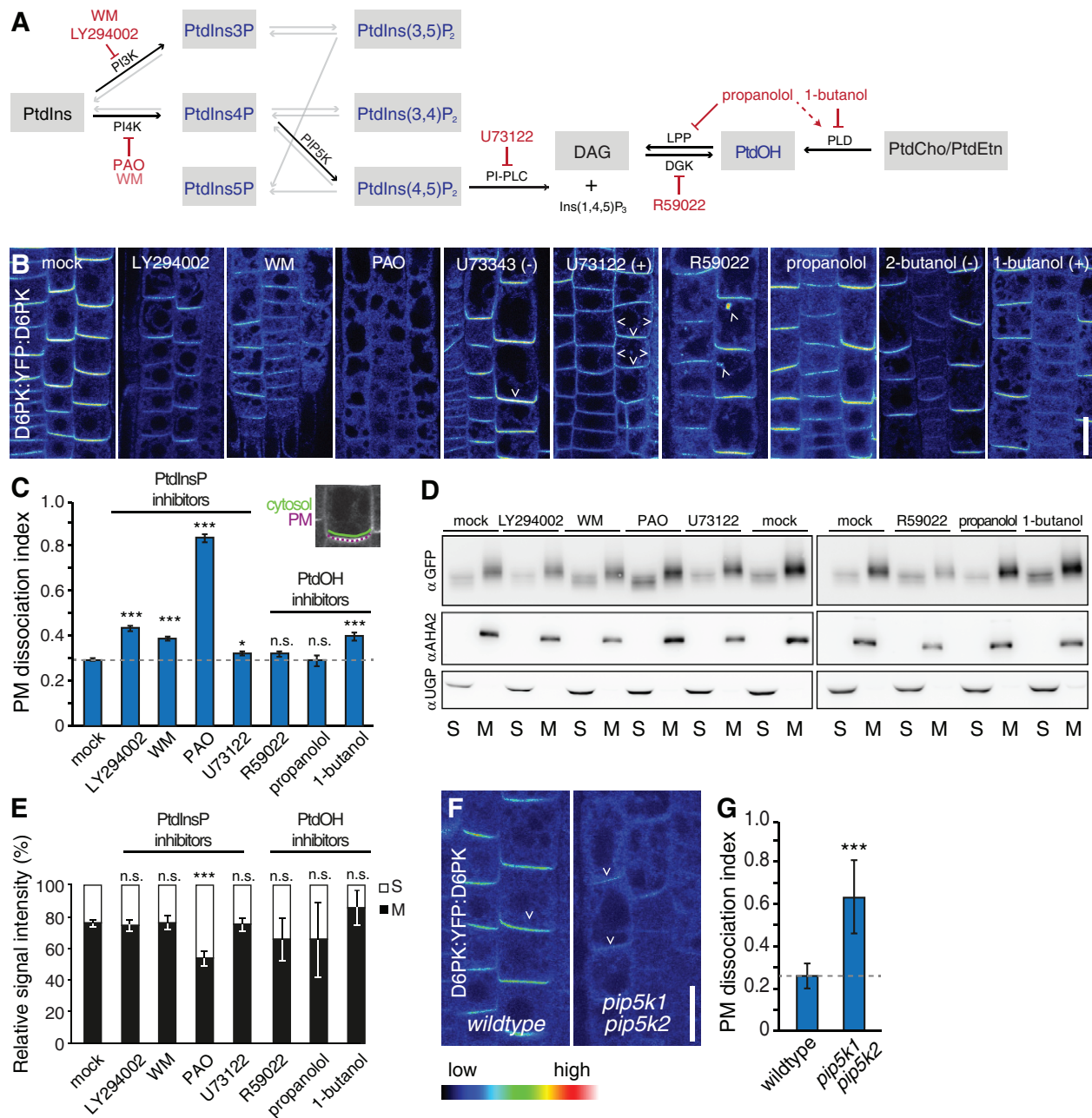
Fig. 2. Phosphoinositide and phosphatidic acid composition determine D6PK recruitment and polarity at the plasma membrane. (A) Scheme of PI and PtdOH biosynthesis pathways and their chemical inhibitors (red). Black arrows, biosynthetic steps analysed in this study; grey arrows, biosynthetic steps that could not be selectively manipulated (Simon et al., 2016; Heilmann, 2009; Meijer and Munnik, 2003; Potocký et al., 2014). Abbreviations (not previously introduced): DAG, diacylglycerol; DGK, DAG KINASE; LPP, LIPID PHOSPHATE PHOSPHATASE; PAO, phenylarsine oxide; PI-PLC, PI-SPECIFIC PHOSPHOLIPASE C; PLD, PHOSPHO-LIPASE D; WM, Wortmannin. (B) Representative confocal images of root epidermis cells from five-day-old D6PK:YFP:D6PK-expressing seedlings treated with inhibitors as specified. All treatments were performed for 30 min in liquid media: mock (0.1% DMSO), WM (33 µM), LY294002 (100 µM), PAO (30 µM), U73343 (−) inactive and U73122 (+) active analogues (5 µM), R59022 (50 µM), propanolol (50 µM), 2-butanol (−) inactive and 1-butanol (+) active analogues (0.8%). Arrows indicate YFP:D6PK at the plasma membrane or endomembranes. All treatments were performed in parallel with the same acquisition parameters and repeated three times with comparable outcomes ($n{\geq}8$ seedlings). Scale bar: 20 µm. (C) Plasma membrane (PM) dissociation index determined as the ratio between the signal detected in the cytosol (solid line in inset image) and at the basal plasma membrane (dashed line in inset image). $n{\geq}40$ epidermal cells from $n{\geq}24$ seedlings. (D) Representative immunoblots with anti-GFP (YFP:D6PK), anti-AHA2 (plasma membrane H+-ATPase; membrane fraction) and anti-UGP (UDP-glucose pyrophosphorylase; soluble fraction) after subcellular fractionation of protein extracts prepared from roots of seven-day-old 35S:YFP:D6PK seedlings treated in the same manner as in B. The effects of the inhibitors on 35S:YFP:D6PK seedlings are similar to those shown in B for D6PK:YFP:D6PK seedlings (Fig. S1). S, soluble supernatant; M, membrane pellet, after 100,000 *g* centrifugation. The experiment was repeated with similar outcomes using three biological replicates. (E) Mean±s.e.m. of the relative abundance of the soluble and membrane fractions determined by densitometric analysis from immunoblots from three biological replicates as shown in D. (F) Representative confocal images of YFP:D6PK in root epidermis cells of seven-day-old wild-type and *pip5k1 pip5k2* seedlings ($n{\geq}6$ seedlings). The semi-quantitative colour-coded heatmap for signal intensities also applies to B. Arrows indicate plasma membrane-associated YFP:D6PK. Scale bar: 20 µm. (G) Plasma membrane (PM) dissociation index from images as shown in F ($n{\geq}40$ cells from six roots). Data in C,G,E represented as mean±s.e.m. *$P{\leq}0.05$; ***$P{\leq}0.001$; n.s., not significant by Student's *t*-test.

YFP-tagged D6PK (YFP:D6PK) in root cells, we examined YFP: D6PK localization and distribution after 30 min treatments with established PI and PtdOH biosynthesis inhibitors (Fig. 2). For comparisons and to establish the effectiveness of the inhibitor treatments, we also analysed the localization of phosphoinositide-specific biosensors, PIN2:GFP trafficking and the uptake of the lipophylic dye and endocytosis tracer FM4-64 (Fig. S1). Interestingly, the PI3-KINASE inhibitors LY294002 and Wortmannin (WM) led to a significant depletion of YFP:D6PK from the plasma membrane (Baggiolini et al., 1987; Simon et al., 2016; Vlahos et al., 1994). Our WM and LY294002 treatments efficiently altered the localization of the PdtIns3P sensor (P18Y) but not of the PdtIns4P (FAPP1) nor PdtIns(4,5)P_2 (P24Y) sensors. With regard to PIN2:GFP, they led to PIN2:GFP accumulation in endosomes, as previously reported for WM treatments, but had no visible effects in overall FM4-64 uptake (Fig. S1) (Jaillais et al., 2006). Conversely, the PI4-KINASE inhibitor PAO caused a strong plasma membrane dissociation of YFP:D6PK (Fig. 2B,C) (Hammond et al., 2012; Simon et al., 2016). As expected, PAO treatment specifically led to the internalization of the PdtIns4P sensor (FAPP1) but, interestingly, also blocked FM4-64 uptake as well as the accumulation of PIN2:GFP in BFA compartments, suggesting that PAO treatment might block endocytosis (Fig. S1). Strikingly, short-term treatments with U73122 (+), an inhibitor of the PI-PLC-mediated hydrolysis of PIs, but not treatments with its inactive analogue U73343 (−), led to a depolarization of YFP:D6PK at the plasma membrane, concomitant with the appearance of the protein in endosomes. Effects on the seemingly polar PdtIns(4,5)P_2 biosensor or on polar PIN2:GFP could not be detected (Fig. 2B,C) (Bleasdale et al., 1990). It is likely that the increased plasma membrane dissociation by the U73122 (+) treatment resulted from the apolar redistribution and consequent reduction of YFP:D6PK signals at the basal plasma membrane where we performed our measurements (Fig. 2B,C). Surprisingly, the subcellular fractionation of protein extracts prepared from roots expressing YFP:D6PK from the 35S CaMV promoter indicated that the observed plasma membrane dissociation after WM, LY294002, PAO, and U73122 treatments was accompanied by an obvious increased solubilization of YFP:D6PK only in the case of the PAO treatment (Fig. 2B-E). For all treatments, we observed similar effects on YFP:D6PK localization, regardless of whether the fusion was expressed from the D6PK or the 35S CaMV promoter (Fig. 2; Fig. S1).

As YFP:D6PK strongly bound to PtdOH, we also tested the effects of the modulation of PtdOH abundance with R59022, an inhibitor of DGK- and PI-PLC-dependent PtdOH synthesis (de Chaffoy de Courcelles et al., 1985; Potocký et al., 2014). R59022 led to the occasional accumulation of YFP:D6PK on endosomes, detectable only when YFP:D6PK was expressed from the D6PK promoter (Fig. 2B; Fig. S1B). Interestingly, PIN2:GFP and FM4-64 also accumulated in R59022-induced compartments (Fig. S1). At the same time, inhibition of PLD-dependent PtdOH production by 1-butanol resulted in the partial internalization of YFP:D6PK, an apparent reduction in FM4-64 uptake as previously reported, but no detectable effects on PIN2:GFP trafficking (Fig. 2B,C; Fig. S1) (Li and Xue, 2007). Conversely, anticipated increases in PtdOH abundance as a result of propanolol treatments had neither an obvious effect on YFP:D6PK localization nor on PIN2:GFP trafficking or FM4-64 uptake (Fig. 2B,C; Fig. S1). Thus, the intracellular levels of PtdOH seemingly regulate YFP:D6PK localization more subtly than PI levels, and likely in a differential manner, depending on whether the PtdOH originates from the PI-PLC or the PLD pathway. Fractionation experiments indicated

that none of the PtdOH inhibitor treatments resulted in the dissociation of YFP:D6PK from cellular membranes (Fig. 2D,E). Taken together, these findings suggested that PtdIns3P, PtdIns(4,5) P_2, and PtdOH, but most importantly PtdIns4P, might be essential for YFP:D6PK plasma membrane localization and also membrane association. By contrast, PtdIns(4,5)P_2 or one of its derivatives might critically determine YFP:D6PK polar distribution.

PIP5K1 and PIP5K2 are required for proper targeting of D6PK
PIP5K1 and PIP5K2, two Arabidopsis PIP5Ks isoforms that convert PtdIns4P to PtdIns(4,5)P_2, preferentially localize to apical and basal domains in root epidermal cells (Ischebeck et al., 2013). As U73122 treatments indicated that PtdIns(4,5)P_2 might control the D6PK membrane association and polarity in root epidermal cells, we introduced the YFP:D6PK transgene into the pip5k1 pip5k2 double mutant. Similarly to the reported internalization of YFP:D6PK in root hair cells of pip5k3 mutants, we noted reduced YFP:D6PK plasma membrane association in the root epidermal cells of the pip5k1 pip5k2 double mutant (Fig. 2F,G) (Stanislas et al., 2015). Thus, the reported alterations of PtdIns(4,5)P_2 levels in pip5k1 pip5k2 mutants might exert an influence on the plasma membrane targeting of D6PK (Ischebeck et al., 2013; Tejos et al., 2014).

The D6PK MID domain is required and sufficient for D6PK plasma membrane anchoring
AGCVIII kinases have an insertion between kinase subdomains VII and VIII that has been implicated in the targeting of different AGCVIII kinases (Rademacher and Offringa, 2012). In the case of D6PK and the orthologous D6PK-LIKE 1 to 3 (D6PKL1-D6PKL3), this insertion is between 101 and 104 amino acids long and designated here as the middle (MID) domain (Fig. 3A). A role of the insertion domain for the specific localization of different AGCVIII kinases has previously been proposed (Ek-Ramos et al., 2010; Zegzouti et al., 2006). In addition, the kinase domains are flanked by N- and C-terminal domains of 117 to 199 amino acids and 45 to 57 amino acids, respectively (Fig. 3A) (Rademacher and Offringa, 2012). To examine the importance of the three domains for D6PK localization, we analysed YFP:D6PK variants lacking these three domains in YFP:D6PKΔN, YFP:D6PKΔMID and YFP: D6PKΔC lines. Conversely, we analysed fusions between YFP and the three isolated domains in YFP:D6PK_N; YFP:D6PK_MID and YFP:D6PK_C lines. The deletion of any of the three domains resulted in the loss of the plasma membrane association of D6PK (Fig. 3B; Fig. S2). Regardless, each of these deletion variants remained associated with membranes, possibly endomembranes (Fig. 3C). Specifically in the case of YFP:D6PKΔMID, an endosomal localization was apparent as judged by its co-localization with the membrane lipid dye FM4-64 (Fig. 3B; Fig. S2). In turn, YFP:D6PK_N and YFP:D6PK_C were neither associated with the plasma membrane nor with membrane fractions after subcellular fractionation (Fig. 3B,C). The MID domain, however, was sufficient to recruit YFP:D6PK_MID to the plasma membrane in a polar manner, albeit with a reduced polarity when compared with YFP:D6PK, and the majority of the protein was identified in the membrane fraction after subcellular fractionation (Fig. 3B-D). Thus, the MID domain is sufficient to mediate the plasma membrane association of D6PK, and to some extent also its polar distribution, but all three domains are required for D6PK plasma membrane association.

The rapid recycling of D6PK from the plasma membrane can be blocked by Brefeldin A (BFA), an inhibitor of the ARF-GEF
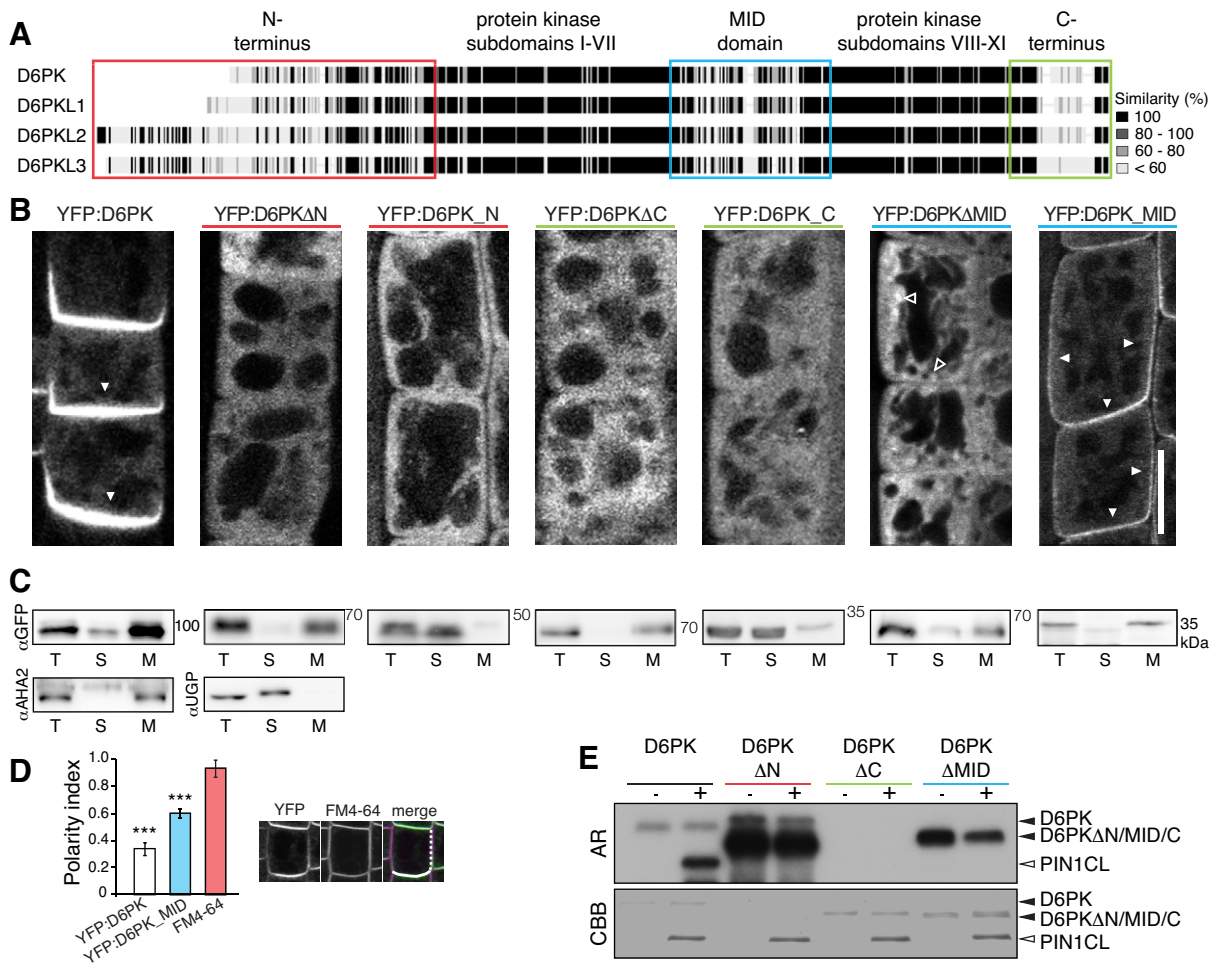
Fig. 3. The MID domain is required and sufficient for D6PK plasma membrane localization. (A) Alignment of D6PK and D6PKLs with amino acid similarities. Frames depict the positions of the analysed domains. (B) Representative confocal images of root meristem epidermal cells from seven-day-old seedlings expressing the specified transgenes under control of the 35S CaMV promoter. Solid arrowheads indicate YFP signals at the plasma membrane; empty arrowheads indicate YFP signals in endomembranes. Scale bar: 10 μm. (C) Representative immunoblots with anti-GFP (YFP:D6PK), anti-AHA2 (plasma membrane H⁺-ATPase; membrane fraction), and anti-UGP (UDP-glucose pyrophosphorylase; soluble fraction) after subcellular fractionation of protein extracts from roots of seven-day-old seedlings as introduced in B. T, total fraction (supernatant after 10,000 g centrifugation); S, soluble supernatant; M, membrane pellet (after 100,000 g centrifugation). (D) Mean±s.e.m. after quantification of the polarity indices, determined as the ratio between average signal intensities of lateral (dashed line in merged image) over basal (solid line in merged image) plasma membranes, from confocal images of roots expressing YFP:D6PK or YFP: D6PK_MID and stained with FM4-64 (2 μM) for 15 min ($n \geq 20$ cells from a total of six roots). Pairwise Student's t-tests were performed between YFP-derived and FM4-64-derived values from respective cells; ***$P \leq 0.001$. (E) Representative autoradiograph (AR) and Coomassie Brilliant Blue (CBB)-stained loading control from *in vitro* kinase assays with recombinant GST:D6PK (D6PK) and GST:D6PK deletion variants (D6PKΔN, D6PKΔC and D6PKΔMID) using GST:PIN1 cytosolic loop (PIN1 CL) as substrate. Loading of D6PKΔN is below the detection limit in the CBB staining but the presence of the kinase is evidenced by the strong activity in the AR.

GNOM (Barbosa et al., 2014; Geldner et al., 2003; Zourelidou et al., 2009). Whereas wild-type YFP:D6PK was observed in intracellular compartments after BFA treatments, no obvious accumulation in BFA-compartments was observed with any of the deletion variants, indicating that their intracellular trafficking might be distinct from that of the BFA-sensitive YFP:D6PK (Fig. S2). Although YFP: D6PK_MID localized to the plasma membrane in a strongly polar manner, the protein was partially insensitive to the effects of BFA (Fig. 3B; Fig. S2). Thus, although the MID domain is sufficient for polar plasma membrane targeting, it displays different recycling and polarity properties from YFP:D6PK.

D6PK is an auto-phosphorylating kinase that trans-phosphorylates PINs (Zourelidou et al., 2014). *In vitro* kinase assays with the PIN1 cytosolic loop showed that D6PKΔN or D6PKΔMID retained the ability for auto-phosphorylation but lost the ability for PIN1 trans-phosphorylation (Fig. 3E). In turn, D6PKΔC had no detectable

auto- or trans-phosphorylation activity (Fig. 3E). This suggested that the N-terminus and the MID domain might be required for PIN substrate recognition or trans-phosphorylation, whereas the C-terminus might be required for D6PK kinase activity. Interestingly, D6PK auto-phosphorylation was increased in D6PKΔN and D6PKΔMID when compared with D6PK, suggesting that the N-terminus and the MID domain might have an inhibitory effect on D6PK kinase activity.

A K-rich motif is required for phospholipid binding and D6PK plasma membrane association

In a search for possible motifs in the MID domain that could confer binding to the plasma membrane, our attention was drawn to a positively charged motif including multiple K and R residues in each of the four D6PK and D6PKL proteins (Fig. 4A) (Hammond and Balla, 2015; Zegzouti et al., 2006). We generated alanine (A)
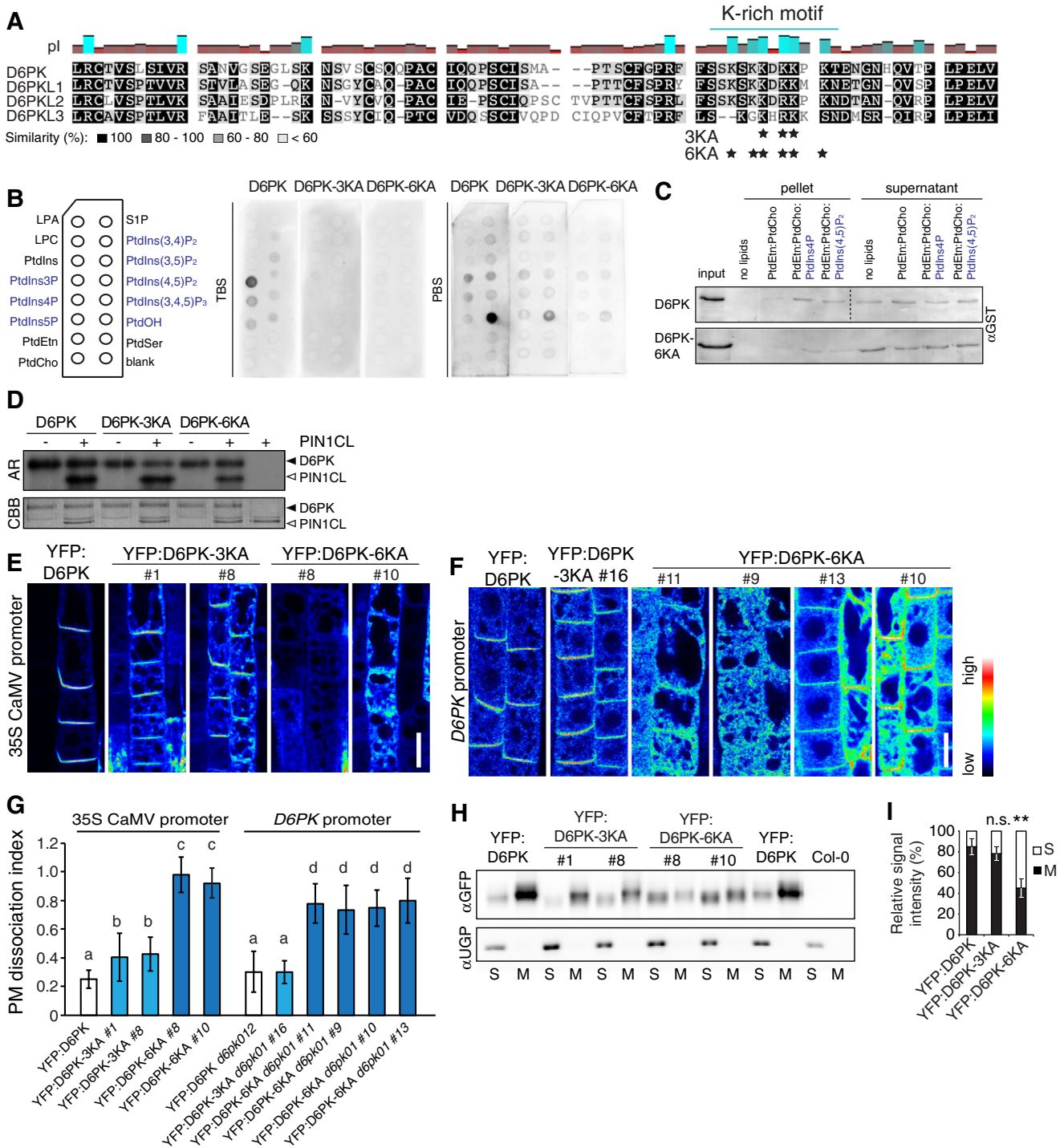
Fig. 4. The K-rich motif in the MID domain is required for D6PK phospholipid binding, membrane association and plasma membrane localization.
(A) Alignment of the D6PK MID domain (amino acids 255 to 335) and the corresponding regions in D6PKLs. Mean isoelectric points (pI) are colour-coded in blue (basic) and red (acidic). Stars depict lysine (K) residues of the K-rich motif substituted by alanine (A) in the YFP:D6PK-3KA and -6KA variants. (B) Representative lipid overlay assay using TRIS and PBS buffers. (C) Anti-GST immunoblot of GST:D6PK and GST:D6PK-6KA after liposome binding assays using lipid mixtures containing the neutral PtdEtn and PtdCho and either the polyacidic PtdIns4P or PtdIns(4,5)P_2 as specified. One of two replicate experiments is shown. All samples from the upper panel are from the same blot; the blot was spliced to eliminate the marker lane (dashed line). (D) Representative AR with the corresponding CBB-stained loading control gel from in vitro kinase assays with recombinant GST:D6PKs and PIN1 CL. (E,F) Confocal images of root meristem epidermal cells of seven-day-old seedlings expressing YFP:D6PK, YFP:D6PK-3KA (3KA) and YFP:D6PK-6KA (6KA) from the 35S CaMV (E) and the D6PK (F) promoters. Numbers of independent T1 transgenic lines are specified. Scale bars: 20 μm. (G) Mean±s.e.m. of the plasma membrane dissociation indices determined from confocal images (n≥45 cells from n≥6 seedlings) similar to those shown in E,F and as specified in Fig. 2. Different letters mark statistically significant differences (P≤0.01), same letters mark statistically non-significant differences by Student's t-test. (H) Representative immunoblots with anti-GFP and anti-UGP (soluble protein control) after subcellular fractionation of total protein extracts prepared from roots of seven-day-old seedlings. (I) Mean±s.e.m. of the relative signal intensities of soluble and membrane fractions measured by densitometric analysis of immunoblots as shown in H from three biological replicates. Student's t-test: **P≤0.01; n.s., not significant.

replacement variants of the three most highly conserved Ks (D6PK-3KA) or all six Ks (D6PK-6KA) in D6PK and found that phospholipid binding was partially (D6PK-3KA) or strongly (D6PK-6KA) impaired in phospholipid binding assays or in liposome binding assays with PtdIns4P or PtdIns(4,5)P_2 (Fig. 4B, C). In turn, these mutations did not affect D6PK auto- or PIN1 trans-phosphorylation (Fig. 4D).

In transgenic plants, the YFP:D6PK-3KA and YFP:D6PK-6KA mutations strongly impaired the plasma membrane association of the protein when expressed from a 35S CaMV promoter in a wild-type Col-0 background (Fig. 4E) or from a *D6PK* promoter fragment in the *d6pk d6pkl1* (*d6pk01*) double mutant (Fig. 4F). The observed intracellular distribution patterns ranged from a partial accumulation in the case of YFP:D6PK-3KA to an almost complete intracellular accumulation of YFP:D6PK-6KA (Fig. 4E-G). In quantitative terms, the effects of the K-to-A mutations on YFP:D6PK plasma membrane association differed depending on the promoter used, where the stronger 35S CaMV promoter led to stronger dissociation indices than the weaker *D6PK* promoter (Fig. 4G). This variation could arise from limiting plasma membrane recruiting factor(s), such as phospholipids or protein, that might become limiting when YFP:D6PK is abundant and presents lower affinity to membranes. In contrast, the individual KA mutants revealed surprisingly conserved dissociation indices between independent transgenic lines with different protein levels, regardless of the promoter driving their expression. For instance, the four *D6PK* promoter lines of YFP:D6PK-6KA with variable absolute signal intensities at the plasma membrane displayed strikingly conserved plasma membrane dissociation indices (Fig. 4F,G).

To test whether absolute protein abundance contributed to the variable plasma membrane abundance of the *D6PK* promoter YFP:D6PK-6KA lines, we analysed total YFP:D6PK abundance from these lines after immunoprecipitations of YFP:D6PK with anti-GFP. We indeed detected a strong accumulation of the YFP:D6PK-6KA protein in lines #13 and #10 with stronger plasma membrane signals, in comparison with the weaker lines #9 and #11 and to YFP:D6PK and YFP:D6PK-3KA lines (Fig. S3A). These differences could not be explained by differences in transcript abundance between these lines (Fig. S3B). We concluded that K residue mutations combined with the resulting localization defects might lead to a disturbance of YFP:D6PK trafficking, protein turnover and ultimately homeostasis.

Owing to the low protein expression levels, we were unable to perform fractionation experiments with lines expressing YFP:D6PK from the *D6PK* promoter. However, when we performed subcellular fractionation experiments with the 35S CaMV promoter-driven YFP:D6PK lines, we detected a shift in the distribution of the protein between the soluble and the membrane fraction in the case of YFP:D6PK-6KA (Fig. 4H,I). Whereas ~80% of YFP:D6PK was retained in the membrane fraction, only ~40% of YFP:D6PK-6KA of the protein resided in the membrane fraction (Fig. 4H,I). In summary, these findings suggest that the K-rich motif of the D6PK MID domain confers the ability to bind to polyacidic phopholipids *in vitro* and to the plasma membrane and endomembranes *in vivo*.
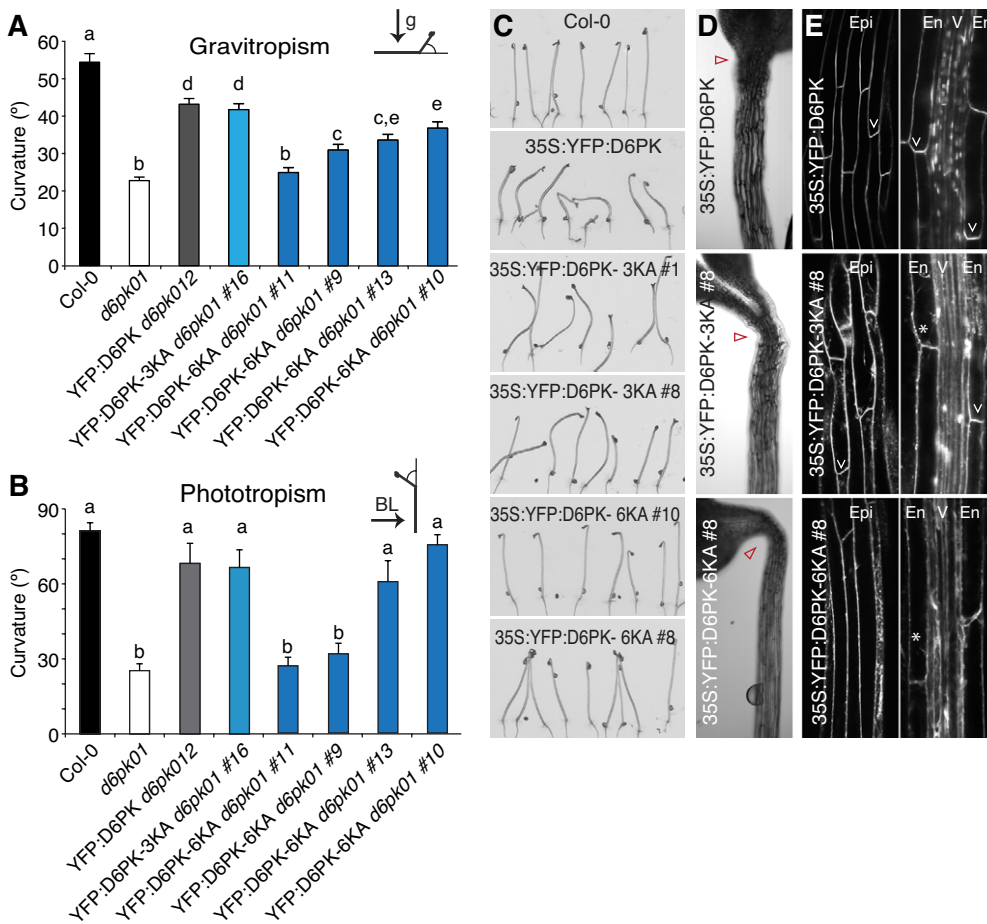
The K-rich motif is required for D6PK function

YFP:D6PK abundance at the plasma membrane is crucial for PIN phosphorylation and auxin transport activation (Barbosa et al., 2014). *d6pk d6pkl1* (*d6pk01*) or *d6pk d6pkl1 d6pkl2* (*d6pk012*) mutants are impaired in auxin transport-dependent growth responses, including negative gravitropism and phototropism of the hypocotyl. Expression of YFP:D6PK from a *D6PK* promoter fragment is sufficient to suppress these phenotypes in *d6pk012*

(Willige et al., 2013). Likewise, YFP:D6PK-3KA, when expressed from the *D6PK* promoter, suppressed the tropism defects of the *d6pk01* mutant efficiently (Fig. 5A,B). However, YFP:D6PK-6KA suppressed *d6pk01* defects less efficiently and the suppression efficiency varied between the individual YFP:D6PK-6KA lines in correlation with their differential tendency to associate with the plasma membrane (Fig. 4, Fig. 5A,B). We therefore suggest that their differential ability to associate with the plasma membrane is the cause for their differential effects in the suppression of the tropism defects of *d6pk01* mutants.

A further indication for an impaired functionality of the proteins came from our analyses of seedlings overexpressing wild-type and mutated YFP:D6PK. Dark-grown seedlings overexpressing YFP:D6PK from the 35S CaMV promoter have strong tropism defects that can be suppressed by treatments with the auxin transport inhibitor N-1-naphthylphthalamic acid (NPA), suggesting that these phenotypes are caused by auxin transport defects (Barbosa et al., 2014). Similarly, the overexpression of YFP:D6PK-3KA, but not that of YFP:D6PK-6KA, caused defects in hypocotyl tropism and apical hook formation that were comparable with, but milder than, those observed after overexpression of wild-type YFP:D6PK (Fig. 5C,D). As in root epidermal cells, we observed a reduction in the plasma membrane signal in YFP:D6PK-3KA and YFP:D6PK-6KA lines in epidermal, endodermal and vascular cells in the hypocotyl when compared with the lines expressing wild-type YFP:D6PK (Fig. 4D, Fig. 5E). Thus, the severity of the overexpression phenotypes in the hypocotyl decreased after mutation of the K-rich motif in line with their differential defects in plasma membrane association and their defects in auxin transport regulation at the plasma membrane.

Proper PIN3 phosphorylation depends on an intact K-rich motif in YFP:D6PK

PIN3 has a role in the control of hypocotyl tropisms and is a direct target of D6PK phosphorylation (Willige et al., 2013; Zourelidou et al., 2014). PIN3 phosphorylation is reduced in *d6pk01* and *d6pk012* (Willige et al., 2013) and BFA treatments, which lead to a dissociation of D6PK from the plasma membrane and impair PIN3 phosphorylation in the wild type (Barbosa et al., 2014). We accordingly expected that the differential accumulation of YFP:D6PK and its mutant variants at the plasma membrane should result in a differential PIN3 phosphorylation. In immunoblots with anti-PIN3, PIN3 can be separated into a slow- and a fast-migrating form, which are better distinguished in intensity profiles (Fig. 6A,B). It was shown that the more slowly migrating form corresponds to a phosphorylated form of PIN3 according to several criteria (Willige et al., 2013). Densitometric analysis revealed that phosphorylated PIN3 was reduced by about 40% in *d6pk01* when compared with the wild type or the *d6pk012* mutant complemented with the wild-type YFP:D6PK transgene. Whereas the complementation of the phosphorylation defect was still efficient with YFP:D6PK-3KA, the degree of complementation was variable between the different YFP:D6PK-6KA lines. Here, the PIN3 phosphorylation defects were partially suppressed in the YFP:D6PK-6KA lines (#13 and #10, Fig. 6), in line with suppression of *d6pk01* tropism defects by YFP:D6PK-6KA in these lines and the fact that they accumulated YFP:D6PK-6KA at the plasma membrane. In turn, PIN3 phosphorylation was not normalized in the YFP:D6PK-6KA lines that could not complement the *d6pk01* phenotype and that had reduced YFP:D6PK-6KA plasma membrane abundance (#9 and #11, Fig. 6 and Fig. 5). Thus, the differential complementation efficiency of the different YFP:D6PK-6KA lines on PIN3

Fig. 5. The K-rich motif is required for proper D6PK function in hypocotyl tropic responses. (A,B) Mean±s.e.m. from a hypocotyl negative gravitropism response after reorientation by 90° for 20 h (A; one representative experiment of three replicates; g, gravity vector) and hypocotyl phototropism response after 4 h of lateral illumination with 5 μmol m^{-2} s^{-1} blue light (B; one representative experiment of three replicates; BL, blue light) of three-day-old etiolated seedlings ($n \geq 30$ seedlings per experiment). Wild-type YFP:D6PK and KA mutant variants were expressed from a D6PK promoter fragment. Student's t-test, different letters mark statistically significant differences ($P<0.05$), same letters mark statistically non-significant differences. (C) Representative photographs of three-day-old etiolated seedlings expressing 35S:YFP:D6PK and 35S:YFP:D6PK-3KA or -6KA. (D) Representative bright-field images of the hypocotyl and apical hook (red arrowhead) of three-day-old etiolated 35S:YFP:D6PK as well as 35S:YFP:D6PK-3KA or -6KA seedlings. (E) Confocal microscopy images of three-day-old etiolated seedlings of the epidermis surface (Epi) and a hypocotyl section depicting the endodermis (En) and vasculature (V). Arrows indicate YFP signals at the plasma membrane; asterisks indicate YFP signals detected in cytoplasmic strands.

phosphorylation correlated with their efficiency to complement *d6pk01* tropism defects and also with their abundance at the plasma membrane (Fig. 4F,G, Fig. 5).

Polybasic motifs are present in many members of the AGCVIII kinase family

D6PK and the three D6PKLs belong to the AGC1 subgroup of the 23-member AGCVIII kinase family of *Arabidopsis* (Rademacher and Offringa, 2012). Besides a number of previously uncharacterized kinases, this family also includes several plasma membrane-resident kinases: the proposed PIN polarity regulators PID, WAG1 and WAG2 (AGC3 subgroup); the blue light receptors PHOTOTROPIN1 (phot1) and phot2 (AGC4 subgroup); and UNICORN (UCN; AGC2 subgroup) (Dhonukshe et al., 2010; Enugutti et al., 2012; Kong et al., 2006; Sakamoto and Briggs, 2002) (Fig. 7). Although all kinases have an insertion corresponding to the D6PK MID domain, the amino acid sequence conservation in this insertion domain and over the K-rich motif of D6PK is rather limited (Fig. 7A). Recently, studies on a biochemically diverse group of proteins from different organisms demonstrated that protein domains required for membrane association could be reliably predicted based on their basic and hydrophobic score (BH score) above a critical threshold value of 0.6 (Bailey and Prehoda, 2015; Brzeska et al., 2010). Accordingly, the biophysical properties, determined by, for example, the BH score rather than amino acid conservation, could control protein-membrane associations. Indeed, when we applied the BH score prediction to D6PK, we identified the K-rich motif with a BH score (0.79) above the critical threshold value (Fig. 7; Fig. S4). Importantly, the 3KA

and 6KA mutations reduced the BH score (<0.6), thus supporting the predictive power of this value (Fig. 7; Fig. S4).

We subsequently surveyed the 23 members of the *Arabidopsis* AGCVIII kinase family for their BH profile and found a peak with BH scores ≥ 0.6 in 18 *Arabidopsis* proteins at the end of the MID domain that coincided, in its relative position, with the D6PK K-rich motif (Fig. 7; Fig. S4). We next tested whether the K/R-enriched motifs were indeed required for plasma membrane association and phospholipid binding in hitherto uncharacterized protein kinases. To this end, we examined the localization of representative members of individual AGC1 family subclades, namely AGC1.3 (BH=0.78), AGC1.7 (0.68), AGC1.8 (0.94) and AGC1.12 (0.8), in their wild-type form and after mutation of the K/R-enriched motifs in protoplasts (Fig. 7B). Conversely, we also tested the binding of wild-type and mutant proteins in lipid overlay assays. In each but one case, the protein kinases associated with the plasma membrane in a polybasic motif-dependent manner (Fig. 7C). A noteworthy exception was AGC1.7, which had the lowest BH score of all proteins tested (0.68) and did not associate with the plasma membrane. All four kinases bound to polyacidic phospholipids with comparable binding specificities in their wild-type form but with visibly reduced affinity in their mutant form, for most of the phospholipids, with the exception of AGC1.8 (Fig. 7C). Thus, the K/R-rich motifs with high BH scores are, in most cases, required for plasma membrane binding and good candidate motifs for phospholipid binding.

DISCUSSION

We have shown that proper phospholipid composition is required for the polar recruitment of D6PK to the plasma membrane and that

DEVELOPMENT
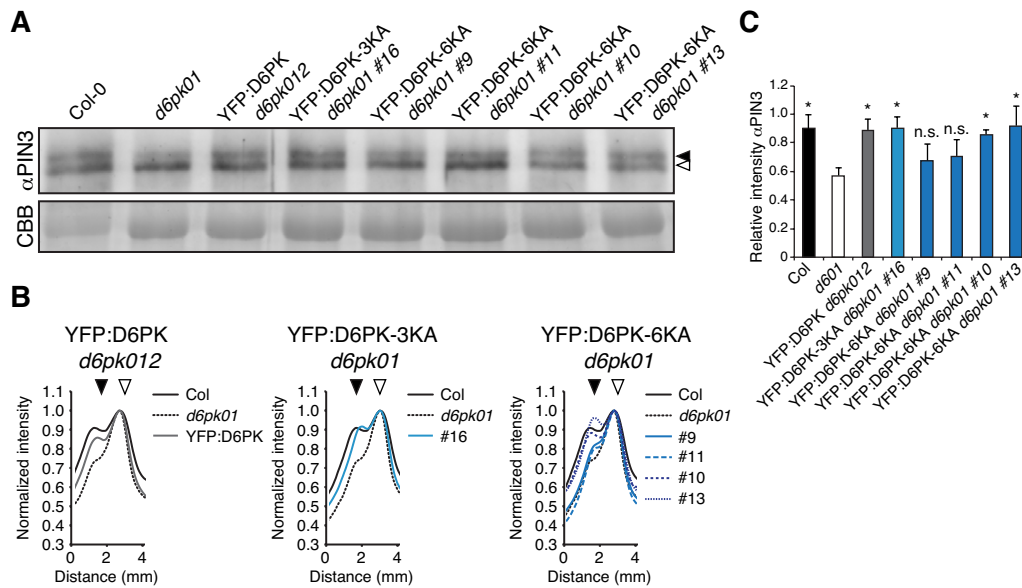
Fig. 6. The K-rich motif is required for proper D6PK-dependent PIN3 phosphorylation at the plasma membrane. (A) Representative anti-PIN3 immunoblot of membrane protein extracts from four-day-old etiolated seedlings and CBB-stained loading control. (B) Densitometric profiles comparing the relative intensities of the upper band, i.e. phosphorylated PIN3 (closed arrowhead), and the lower band, i.e. unphosphorylated PIN3 (open arrowhead) of the different complementation lines from the blot shown in A. Intensity values were normalized to the maximum value of the lower band intensity value. (C) Mean±s.d. of the ratios between the anti-PIN3 upper and lower band intensities from three biological replicates. Student's t-test in relation to the d6pk01 mutant; *$P \leq 0.05$; n.s., not significant.

a K-rich motif in the D6PK MID domain mediates protein-phospholipid interactions. We propose that phospholipid metabolism determines the plasma membrane composition and polar distribution of negatively charged phospholipids that recruit D6PK via its positively charged K-rich motif (Fig. 8). In line with this, we find that mutations of the K-rich motif impair D6PK membrane association and auxin transport-dependent tropic responses that correlate with defects in the phosphorylation of the auxin efflux carrier PIN3.

In *in vitro* binding assays, D6PK could bind to polyacidic PIs and PtdOH in a K-rich motif-dependent manner. *In vivo* manipulation of PI or PtdOH metabolism led to the intracellular accumulation of YFP:D6PK and impaired its polar plasma membrane distribution but only manipulation of PtdIns4P synthesis affected YFP:D6PK solubility. At the same time, K-rich motif mutations in D6PK led to increased solubilization of the protein. This suggests that the intact K-rich domain is required for interactions with polyacidic phospholipids in different membranes and that the specific phospholipid composition in a given membrane might determine D6PK recruitment to different membranes. The D6PK interaction with multiple polyacidic phospholipids through ionic interactions resembles previously reported mechanisms for protein-phospholipid ionic interactions and is distinct from interactions mediated between phospholipids and globular protein domains (Hammond and Balla, 2015; Li et al., 2014).

PtdOH biosensors have indicated that PtdOH is enriched at the apical and sub-apical plasma membranes in pollen tubes (Potocký et al., 2014; Simon et al., 2014). Interestingly, the same manipulations that affected the behaviour of a PtdOH biosensor in pollen tubes also affected the intracellular distribution of D6PK in root cells, i.e. the inhibition of PLD by 1-butanol resulted in the internalization of both proteins and inhibition of DGK by R59022 resulted in the accumulation of both proteins in endosomal compartments. PtdOH is thus a good candidate phospholipid for anchoring D6PK at the plasma membrane.

PI-kinases and phosphatases determine the abundance of different PI species in different membranes; PI biosensors indicate that PtdIns4P and PtdIns(4,5)P$_2$ reside in the plasma membrane whereas PtdIns3P resides in the late endosomes and the tonoplast. In turn, genetic evidence indicates that PtdIns(3,5)P$_2$ might be produced at the tonoplast and late endosomes (Heilmann and Heilmann, 2015; Hirano et al., 2015; Novakova et al., 2014; Simon et al., 2014, 2016; Vermeer et al., 2006, 2009). The cellular distribution of PtdIns5P in plants is unknown and neither PtdIns(3,4)P$_2$ nor PtdIns(3,4,5)P$_3$ have as yet been detected in plants (Heilmann, 2009; Munnik and Nielsen, 2011). In our experiments, treatments with WM and LY294002, which are expected to result in the depletion of PtdIns3P (WM and LY294002) and PtdIns4P (only WM), caused D6PK internalization but did not affect D6PK membrane association. As PtdIns3P has not yet been detected at the plasma membrane, the effects at least of WM but not of LY294002 on D6PK plasma membrane localization could be caused by the plasma membrane depletion of PtdIns4P or other indirect effects on membrane or protein trafficking. A recent study supports this hypothesis by demonstrating that PtdIns4P is the predominant phospholipid in plant plasma membranes and that the AGCVIII kinase PID localizes to the plasma membrane in a PtdIns4P-dependent manner (Simon et al., 2016).

The U73122-mediated inhibition of PtdIns(4,5)P$_2$ hydrolysis led to a quick depolarization of D6PK. This resembled the U73122-induced depolarization of a tip-localized PtdIns(4,5)P$_2$ biosensor in pollen tubes, which was observed after inhibition of PI-PLCs with subapical lateral localization (Helling et al., 2006; Zhao et al., 2010). The observed depolarization of YFP:D6PK suggests that PtdIns(4,5)P$_2$ is also polarized in root epidermal cells. There is, however, still some controversy as to whether the PtdIns(4,5)P$_2$ biosensor has an apicobasal localization in these cells (Ischebeck et al., 2013; Simon et al., 2016; Tejos et al., 2014). Regardless, it is tempting to speculate that U73122 treatment blocks a lateral PI-PLC function in the root epidermis, which could
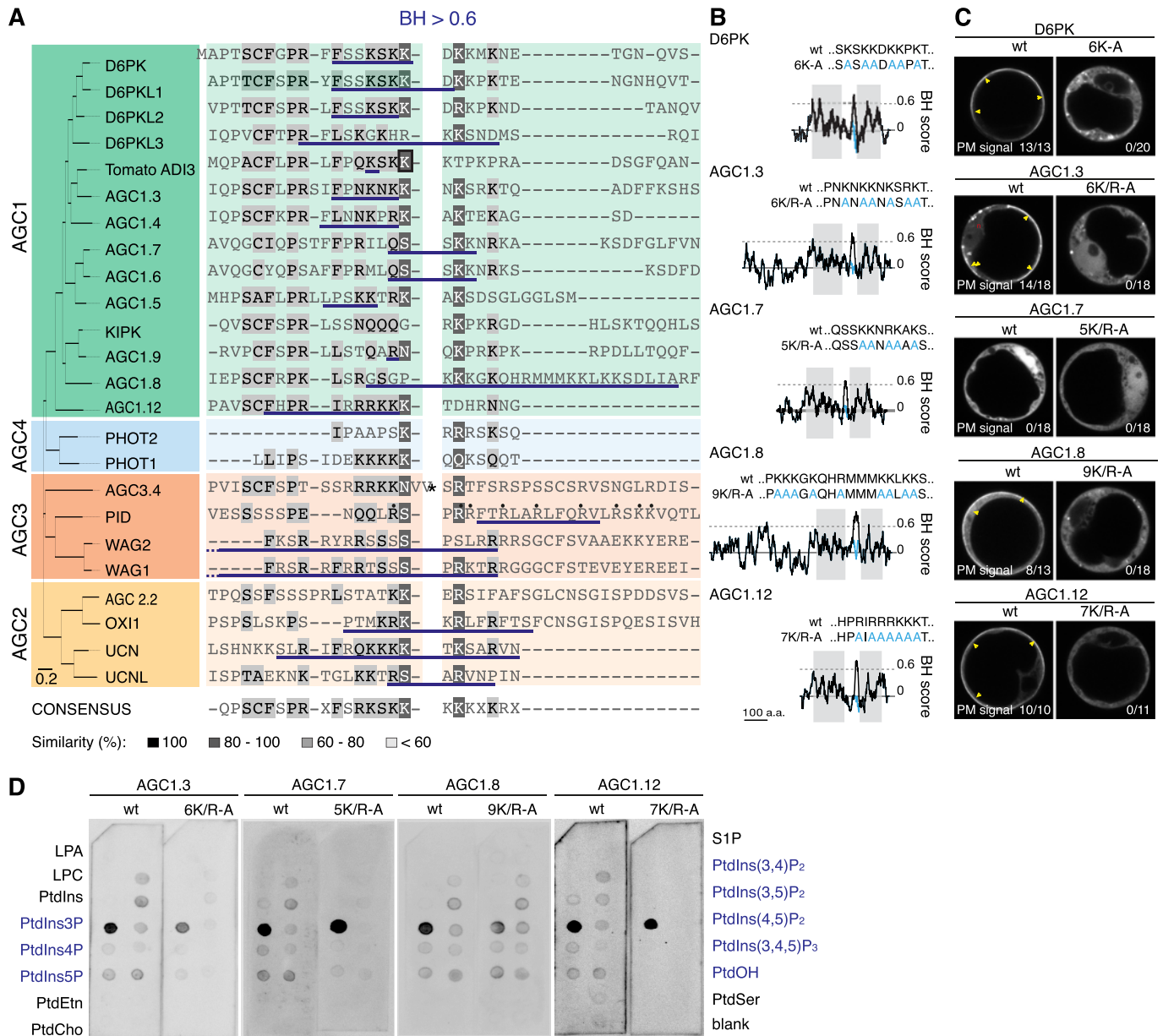
Fig. 7. Basic hydrophobic motifs mediate plasma membrane association and phospholipid binding in several *Arabidopsis* AGC1 kinases.
(A) Phylogenetic tree and alignment of the 23 *Arabidopsis* AGCVIII kinases and the tomato AGCVIII kinase ADI3 using full-length protein sequences (Cost matrix, Blosum62; gap open penalty, 12; gap extension penalty, 3). Shown is the part of the alignment corresponding to the D6PK K-rich motif and the corresponding regions with a BH score >0.6 (blue underlined) for each kinase. Dots mark amino acids mutated in a recent study on PID (Simon et al., 2016). A 23-amino acid stretch was deleted from AGC3.4 (*) as it disturbed the alignment; its BH score was calculated for the entire region. (B) BH score profiles of AGC1.3, AGC1.7, AGC1.8 and AGC1.12. The profiles of the wild-type (black) and the K/R-motif-mutated protein (blue) were overlaid. Shadowed areas indicate the positions of the two protein kinase subdomains I to VII (left) and VIII to XI (right). Wild-type (black) and mutated (blue) sequences are shown. (C) Representative images of protoplasts expressing wild-type and mutant YFP-tagged kinases. The frequency of protoplasts with plasma membrane localization is specified. Yellow arrowheads mark some areas of plasma membrane localization. (D) Representative images from two technical replicates of lipid overlay assays with recombinant GST-tagged kinases (TRIS-buffer). The corresponding blots were exposed simultaneously to ensure comparable exposure conditions. For abbreviations see Fig. 1 legend.

then lead to a depolarization of PtdIns(4,5)P$_2$ and D6PK, and that the current PtdIns(4,5)P$_2$ biosensor fails to recapitulate the PI dynamics. Future dissection of the polarity functions of PI4P 5-kinases and PI-PLCs in the root epidermis will be required to examine this hypothesis.

As almost all of our (short-term) manipulations of PI and PtdOH biosynthesis had an impact on D6PK localization, with the strongest effects following the PAO-induced depletion of PtdIns4P, we

suggest that not only one particular phospholipid but rather a combination of PtdOH and PIs might be responsible for D6PK plasma membrane recruitment. The retention of a weak but detectable plasma membrane association in the D6PK-3KA and -6KA variants or with a deletion of the MID domain suggests that there are other determinants of membrane association within D6PK. Alternatively, regions other than the D6PK MID domain might mediate additional interactions with membrane proteins or
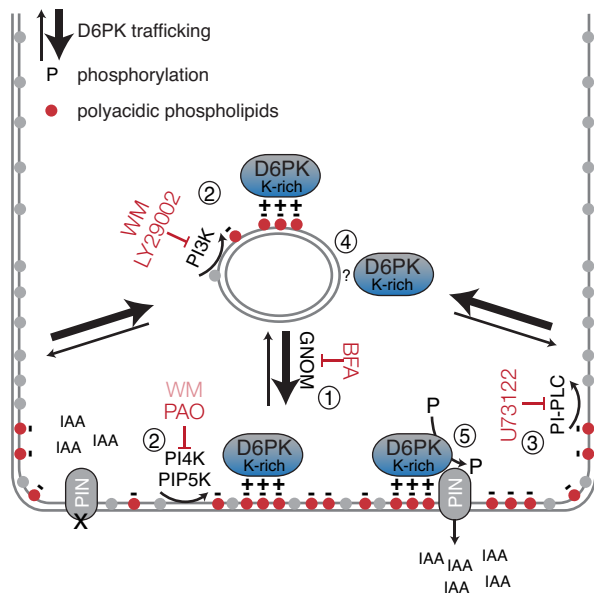
Fig. 8. Model for D6PK recruitment, polarity control and activation of PIN-mediated auxin transport at the plasma membrane. D6PK polar localization is controlled by dynamic phospholipid metabolism, the affinity of D6PK to polyacidic phospholipids through its K-rich motif and the dynamic targeting to and removal from the plasma membrane (recycling). (1) Targeting of D6PK to the plasma membrane is GN dependent and BFA sensitive, suggesting that it is mediated by vesicle-mediated transport (Barbosa et al., 2014). (2) At the plasma membrane, D6PK binds to polyacidic phospholipids such as PtdOH, PtdIns4P and PtdIns(4,5)P_2 (red dots) through ionic interactions with its K-rich motif. When internalized, D6PK might also bind intracellular membranes through other polyacidic phospholipids, e.g. PtdIns3P (red dots). Impairment of PI biosynthesis using inhibitors or *pip5k* mutants leads to the dissociation of D6PK from the plasma membrane and possibly binding to endomembranes. (3) Accumulation of the presumably polar PtdIns(4,5)P_2 after inhibition of lateral PI-PLC enzymes (U73122), leads to depolarization of D6PK, suggesting that the D6PK polarity domain is restricted by basal PIP5K-PtdIns(4,5)P_2 and lateral PI-PLC modules. (4) D6PK membrane association is not exclusively controlled through the K-rich motif. (5) D6PK phosphorylates and activates PINs and polar auxin transport only at the plasma membrane. IAA (indole-3-acetic acid), auxin.

phospholipids, or yield lipid modifications required for D6PK affinity and specificity to membranes. Such a coincident detection has been often described for the recruitment of peripheral membrane proteins (Carlton and Cullen, 2005; Hammond and Balla, 2015; Stahelin et al., 2014). Importantly, we can exclude that kinase activity might control D6PK localization, as we have previously shown that inactive YFP:D6PK maintains similar polarity and recycling kinetics to the wild-type protein (Barbosa et al., 2014).

Despite limited sequence similarity in the insertion domain, many AGCVIII protein kinases have a high BH score, specifically in the region corresponding to the D6PK K-rich motif. We thus propose, and have in part tested, that these other kinases are recruited to the plasma membrane (and possibly internal membranes) through similar mechanisms to those studied in detail for D6PK. While this study was in progress, an analysis of the mechanisms targeting the AGCVIII kinase PID to the plasma membrane identified the corresponding motif in PID to be required for PID plasma membrane association (Simon et al., 2016). Although the BH score might allow prediction of membrane associations, slight differences in motif length and features of nearby residues, e.g. hydrophobicity or phosphorylation, might affect their properties with regard to phospholipid specificity,

membrane localization or trafficking as reported for other proteins (Schmick et al., 2014; Yeung et al., 2008). For example, the K/R-rich motif in the middle domain of the D6PK-related ADI3 kinase from tomato determines its dual targeting between nucleus and endomembranes (Ek-Ramos et al., 2010, 2014; Heo et al., 2006; Maures et al., 2011). Similar mechanisms might control the distribution of D6PK between the plasma membrane and endomembranes, or even the nucleus, and the existence of such mechanisms might also explain the differential localization of AGC1.7 in our protoplast studies.

In summary, we propose a model for D6PK plasma membrane anchoring and polarity maintenance where both the phospholipid composition of the plasma membrane and the D6PK surface charge at the K-rich motif of the MID domain critically determine D6PK plasma membrane steady-state levels (Fig. 8). This model provides a basis for the involvement of phospholipids in the control of auxin transport activity, and possibly directionality, by D6PK plasma membrane abundance and distribution. The findings reported here for D6PK might also be relevant for the other, as yet uncharacterized, AGC family kinases or other membrane-associated proteins with a high BH score.

MATERIALS AND METHODS
Biological material
The following previously published *Arabidopsis thaliana* mutants and transgenic lines in the Columbia-0 background were used in this study: *d6pk d6pkl1* double mutants (*d6pk01*) (Zourelidou et al., 2009), *pip5k1 pip5k2* double mutants (Ischebeck et al., 2013), 35S:YFP:D6PK in the wild-type background and D6PK:YFP:D6PK in the *d6pk d6pkl1 d6pkl2* background (D6PK *d6pk012*) (Willige et al., 2013; Zourelidou et al., 2009), PIN2:PIN2:GFP (PIN2:GFP) (Abas et al., 2006), as well as the phosphoinositide marker lines P18Y (2xFYVE[HRS]) for PtdIns3P, YFP-PH[FAPP1] for PtdIns4P, and P24Y (2xPH[PLC]) for PtdIns(4,5)P_2 (Simon et al., 2014; Vermeer et al., 2009).

Cloning procedures
Clones of D6PK protein domain variants were obtained by PCR-amplification of Gateway-compatible PCR fragments from pDONR201 (Life Technologies) containing the D6PK coding sequence (Zourelidou et al., 2009) with the following primers: IB2 and IB3 for YFP:D6PKΔN (amino acids 109 to 499); IB1 and IB4 for YFP:D6PK_N (amino acids 1 to 108); IB1 and IB5 for YFP:D6PKΔC (amino acids 1 to 446); IB2 and IB6 for YFP:D6PK_C (amino acids 447 to 499); IB7 and IB8 for YFP:D6PK_MID (amino acids 255 to 335). The PCR fragments were then inserted into the entry vector pDONR201. YFP:D6PKΔMID, with a deletion of amino acids 255 to 355, was obtained by *Sac*I digestion and re-ligation of a pDONR-D6PK clone, which had been mutagenized with the primers IB9 and IB10 to introduce *Sac*I sites flanking the MID domain. To generate the D6PK-3KA variant, lysines K315, K317 and K318 were replaced by alanines in pDONR-D6PK using site-directed mutagenesis with the primer IB70. For the D6PK-6KA mutant variant, lysines K312, K314 and K320 were mutated in D6PK-3KA with IB62. All primer sequences are listed in Table S1.

Inserts of the pDONR201 entry clones with the above-described deletions or mutations were introduced into the destination vectors pDEST15 (Life Technologies) to obtain glutathione-S-transferase (GST) N-terminal fusion constructs for recombinant expression in bacteria or into pEXTAG-YFP-GW to generate constructs for the expression of N-terminal YFP-fusions under control of the 35S CaMV promoter in plants. D6PK mutant variants were also excised as *Xho*I/*Not*I fragments from the pEXTAG-YFP-GW vectors and inserted into a pGREEN0229 vector derivative containing a *D6PK* promoter sequence and a 35S CaMV terminator sequence (Zourelidou et al., 2014). All pEXTAG-YFP-GW overexpression constructs were transformed by floral dip into the wild type (Col-0) and all pGREEN0229 constructs were transformed into *d6pk01* for complementation analysis (Clough and Bent, 1998).

The open-reading frames of AGC1.3, AGC1.7, AGC1.8 and AGC1.12 were amplified by PCR and inserted via pDONR201 into the destination vectors pDEST15 (Life Technologies) to obtain GST N-terminal fusion constructs for recombinant expression in bacteria or into pEXTAG-YFP-GW to generate constructs for the expression of N-terminal YFP fusions under control of the 35S CaMV promoter in plants. Polybasic motifs were mutated using overlap extension PCRs with complementary mutated primers (Hansson et al., 2008). In the case of AGC1.8, this PCR was performed in two rounds due to the extended length of the polybasic motif. Protoplast transformation was performed as previously described (Katsiarimpa et al., 2011). Confocal analysis was carried out 14 h after transformation. All primer sequences are listed in Table S1.

Inhibitor treatments and confocal microscopy

Unless otherwise stated, seedlings for microscopic analyses were grown in continuous white light (110 µmol/m^{-2} s^{-1}) at 21°C for 5-7 days on ½ MS medium (2.15 g/l Murashige and Skoog salts, 0.5 g/l 2-N-morpholino ethane-sulfonic acid, 8 g/l agar, pH 5.8). The following inhibitors were dissolved in DMSO and used as previously described: Wortmannin (Applichem) (Jaillais et al., 2006); LY294002 (Sigma) (Simon et al., 2016); PAO (Sigma) (Simon et al., 2016); U73343 and U73122 (Sigma) (Andreeva et al., 2010; Zhao et al., 2010); R59022 (Sigma) (Li and Xue, 2007; Potocký et al., 2014); propanolol (Sigma) (Li and Xue, 2007; Potocký et al., 2014); 1- and 2-butanol (Sigma) (Li and Xue, 2007; Potocký et al., 2014); Brefeldin A (Fischer Scientific) (Barbosa et al., 2014). All inhibitor treatments were controlled by solvent control treatments performed in parallel. FM4-64 (2 µM) staining was performed as described in the figure legends. All confocal images were acquired with an Olympus FV1000 confocal microscope with high-sensitivity GaAsP detectors using identical acquisition settings between samples (Olympus). Image analyses and quantification were performed using Fiji and as further specified in the results sections and figure legends (Schindelin et al., 2012).

Phospholipid binding assays

For lipid binding assays, GST fusion proteins were recombinantly expressed in *Escherichia coli* BL21(DE3) and purified using Glutathione Sepharose 4B (GE Healthcare). Free GST protein was expressed from pGEX-6P-1 (GE Healthcare) as a negative control. Lipid overlay assays using PIP-strips were performed following manufacturer's instructions (Echelon). In brief, membranes were blocked overnight at 4°C in a blocking buffer with 4% BSA either in TBS-T (0.1% Tween) or PBS-T (0.1% Tween). Purified proteins (0.5 µg/ml blocking buffer) were incubated with PIP-strip membranes for 1 h at room temperature, washed three times for 10 min with TBS-T or PBS-T, then incubated for 1 h with anti-GST (1:2000 in blocking buffer; GE Healthcare), washed three times and incubated for 1 h at room temperature with anti-goat peroxidase conjugate antibodies (1:8000 in blocking buffer; Sigma, A5420). After three final washes, detection of bound proteins was performed using Pierce ECL Plus Western Blotting Substrate (Thermo Scientific) in a Fujifilm LAS 4000 Mini (Fuji).

Liposome binding assays were performed as previously described (Julkowska et al., 2013). Liposomes were prepared from 400 nmol of total lipids at the following molar ratios: PtdCho:PtdEtn, 1:1; PtdCho:PtdEtn:PtdIns4P, 2:2:1; PtdCho:PtdEtn:PtdIns(4,5)P$_2$, 2:2:1; PtdCho:PtdEtn:PtdOH, 2:2:1. All lipids were obtained from Avanti Polar Lipids. Proteins were separated by 10% SDS-PAGE and blotted to Protran nitrocellulose membranes (GE Healthcare). GST-tagged D6PK and D6PK-6KA were detected with goat anti-GST (GE Healthcare, 27457701V) and visualized using a rabbit anti-goat antiserum conjugated to an alkaline phosphatase reporter (Sigma).

In vitro kinase assays were performed with purified recombinant kinases using GST:PIN1 CL (cytosolic loop) as a phosphorylation substrate (Zourelidou et al., 2009). Equal protein amounts (~0.5 µg) were incubated for 60 min at 28°C in a buffer [25 mM Tris-HCl pH 7.5, 5 mM MgCl$_2$, 0.2 mM EDTA, 50 µM ATP, 1× Complete Protease Inhibitor Cocktail (Roche)] supplemented with 10 µCi [γ-^{32}P]-ATP [370 MBq, specific activity 185 TBq (Hartmann Analytic)]. Reactions were stopped by adding 5× Laemmli buffer, samples were then boiled and separated in two SDS-PAGE gels, one for autoradiography and one for staining with Coomassie Brilliant Blue as a loading control.

Negative gravitropism and phototropism responses

Seedlings were grown for 2.5 days on ½ MS in the dark. Two hours before the experiment, agravitropically growing seedlings were straightened under green safe light. For phototropism response experiments, etiolated seedlings were transferred to a FloraLED chamber (CLF Plant Climatics) and illuminated for 4 h with 5 µmol m^{-2} s^{-1} unilateral blue light. For the hypocotyl negative gravitropism response experiments, plates were reoriented by 90° and kept in the dark for an additional 20 h. Plates were scanned and bending angles were quantified using Fiji (Schindelin et al., 2012).

Immunoblots

For the detection of YFP-tagged D6PK and its variants, roots of seven-day-old seedlings were homogenized with protein extraction buffer (PEB; 50 mM Tris-HCl pH 7.5, 150 mM NaCl, 0.1 mM MG132, 0.1 mM PMSF, 1% (v/v) Protease Inhibitor Cocktail (Sigma), and PhosStop phosphatase inhibitor cocktail (Roche)]. For fractionation experiments, extracts were pre-cleared by centrifugation at 10,000 *g* and the supernatant (T) was subsequently ultra-centrifuged at 100,000 *g* to yield the soluble (S) and membrane (M) fractions. Membrane fractions were resuspended in the same volume as soluble fractions with PEB. Samples were denatured with 1× Laemmli buffer and heated at 42°C for 15 min. For immunoblotting, the equivalent of 10 µg total protein was separated on a 10% SDS-PAGE and transferred to nitrocellulose membrane (GE Healthcare) by semi-dry blotting. Immunoblots were detected with rabbit anti-GFP (1:3000; Fischer Scientific, A11122) and rabbit anti-UGP (1:2000; Agrisera, AS05086) and secondary antibody goat anti-rabbit HRP (1:2000; Sigma, A9169). Chemiluminescence detection was performed with a Fujifilm LAS 4000 Mini, total band and band profile intensities were quantified using the Fujifilm Multi Gauge v3.0 software.

For immunoprecipitation, protein was extracted in PEB with 0.5% Triton X-100 from seven-day-old seedlings and subsequently diluted to reduce the Triton X-100 concentration to 0.01%. YFP:D6PK was then immunoprecipitated from 3 mg protein extract with 15 µl GFP-Trap_MA slurry (Chromotek) for 1 h at 4°C. Subsequent wash steps followed the manufacturer's protocol. Beads were resuspended in 40 µl 2× Laemmli buffer and 10 µl were used for SDS-PAGE and immunoblotting as described above. A 5 µg aliquot of total protein extract (input) was used for SDS-PAGE and immunoblotting with anti-UGP as a loading control.

For PIN3 immunoblots, protein extraction, quantification and profile analysis was performed using four-day-old dark-grown seedlings as previously described (Barbosa et al., 2014; Willige et al., 2013).

qRT-PCR analyses

RNA extraction and qRT-PCR analysis were performed as previously described (Lutz et al., 2015). Primer sequences are provided in Table S1.

DEVELOPMENT

Supplementary information
Supplementary information available online at
http://dev.biologists.org/lookup/doi/10.1242/dev.137117.supplemental

References

Abas, L., Benjamins, R., Malenica, N., Paciorek, T., Wiřniewska, J., Moulinier-Anzola, J. C., Sieberer, T., Friml, J. and Luschnig, C. (2006). Intracellular trafficking and proteolysis of the Arabidopsis auxin-efflux facilitator PIN2 are involved in root gravitropism. *Nat. Cell Biol.* **8**, 249-256.

Adamowski, M. and Friml, J. (2015). PIN-dependent auxin transport: action, regulation, and evolution. *Plant Cell* **27**, 20-32.

Andreeva, Z., Barton, D., Armour, W. J., Li, M. Y., Liao, L. F., McKellar, H. L., Pethybridge, K. A. and Marc, J. (2010). Inhibition of phospholipase C disrupts cytoskeletal organization and gravitropic growth in Arabidopsis roots. *Planta* **232**, 1263-1279.

Baggiolini, M., Dewald, B., Schnyder, J., Ruch, W., Cooper, P. H. and Payne, T. G. (1987). Inhibition of the phagocytosis-induced respiratory burst by the fungal metabolite wortmannin and some analogues. *Exp. Cell Res.* **169**, 408-418.

Bailey, M. J. and Prehoda, K. E. (2015). Establishment of Par-polarized cortical domains via phosphoregulated membrane motifs. *Dev. Cell* **35**, 199-210.

Balla, T. (2013). Phosphoinositides: tiny lipids with giant impact on cell regulation. *Physiol. Rev.* **93**, 1019-1137.

Barbosa, I. C. R. and Schwechheimer, C. (2014). Dynamic control of auxin transport-dependent growth by AGCVIII protein kinases. *Curr. Opin. Plant Biol.* **22**, 108-115.

Barbosa, I. C. R., Zourelidou, M., Willige, B. C., Weller, B. and Schwechheimer, C. (2014). D6 PROTEIN KINASE activates auxin transport-dependent growth and PIN-FORMED phosphorylation at the plasma membrane. *Dev. Cell* **29**, 674-685.

Behnia, R. and Munro, S. (2005). Organelle identity and the signposts for membrane traffic. *Nature* **438**, 597-604.

Bleasdale, J. E., Thakur, N. R., Gremban, R. S., Bundy, G. L., Fitzpatrick, F. A., Smith, R. J. and Bunting, S. (1990). Selective inhibition of receptor-coupled phospholipase C-dependent processes in human platelets and polymorphonuclear neutrophils. *J. Pharmacol. Exp. Ther.* **255**, 756-768.

Brzeska, H., Guag, J., Remmert, K., Chacko, S. and Korn, E. D. (2010). An experimentally based computer search identifies unstructured membrane-binding sites in proteins: application to class I myosins, PAKS, and CARMIL. *J. Biol. Chem.* **285**, 5738-5747.

Carlton, J. G. and Cullen, P. J. (2005). Coincidence detection in phosphoinositide signaling. *Trends Cell Biol.* **15**, 540-547.

Cho, W. and Stahelin, R. V. (2005). Membrane-protein interactions in cell signaling and membrane trafficking. *Annu. Rev. Biophys. Biomol. Struct.* **34**, 119-151.

Clough, S. J. and Bent, A. F. (1998). Floral dip: a simplified method for Agrobacterium-mediated transformation of Arabidopsis thaliana. *Plant J.* **16**, 735-743.

Comer, F. I. and Parent, C. A. (2007). Phosphoinositides specify polarity during epithelial organ development. *Cell* **128**, 239-240.

de Chaffoy de Courcelles, D. C., Roevens, P. and Van Belle, H. (1985). R 59 022, a diacylglycerol kinase inhibitor. Its effect on diacylglycerol and thrombin-induced C kinase activation in the intact platelet. *J. Biol. Chem.* **260**, 15762-15770.

de Reuille, P. B., Bohn-Courseau, I., Ljung, K., Morin, H., Carraro, N., Godin, C. and Traas, J. (2006). Computer simulations reveal properties of the cell-cell signaling network at the shoot apex in Arabidopsis. *Proc. Natl. Acad. Sci. USA* **103**, 1627-1632.

Dhonukshe, P., Huang, F., Galvan-Ampudia, C. S., Mähönen, A. P., Kleine-Vehn, J., Xu, J., Quint, A., Prasad, K., Friml, J., Scheres, B. et al. (2010). Plasma membrane-bound AGC3 kinases phosphorylate PIN auxin carriers at TPRXS(N/S) motifs to direct apical PIN recycling. *Development* **137**, 3245-3255.

Ding, Z., Galván-Ampudia, C. S., Demarsy, E., Łangowski, L., Kleine-Vehn, J., Fan, Y., Morita, M. T., Tasaka, M., Fankhauser, C., Offringa, R. et al. (2011). Light-mediated polarization of the PIN3 auxin transporter for the phototropic response in Arabidopsis. *Nat. Cell Biol.* **13**, 447-452.

Ek-Ramos, M. J., Avila, J., Cheng, C., Martin, G. B. and Devarenne, T. P. (2010). The T-loop Extension of the tomato protein kinase AvrPto-dependent Pto-interacting protein 3 (Adi3) directs nuclear localization for suppression of plant cell death. *J. Biol. Chem.* **285**, 17584-17594.

Ek-Ramos, M. J., Avila, J., Nelson Dittrich, A. C., Su, D., Gray, J. W. and Devarenne, T. P. (2014). The tomato cell death suppressor Adi3 is restricted to the endosomal system in response to the *Pseudomonas syringae* effector protein AvrPto. *PLoS ONE* **9**, e110807.

Enugutti, B., Kirchhelle, C., Oelschner, M., Torres Ruiz, R. A., Schliebner, I., Leister, D. and Schneitz, K. (2012). Regulation of planar growth by the Arabidopsis AGC protein kinase UNICORN. *Proc. Natl. Acad. Sci. USA* **109**, 15060-15065.

Feraru, E., Feraru, M. I., Kleine-Vehn, J., Martiniere, A., Mouille, G., Vanneste, S., Vernhettes, S., Runions, J. and Friml, J. (2011). PIN polarity maintenance by the cell wall in Arabidopsis. *Curr. Biol.* **21**, 338-343.

Friml, J., Yang, X., Michniewicz, M., Weijers, D., Quint, A., Tietz, O., Benjamins, R., Ouwerkerk, P. B. F., Ljung, K., Sandberg, G. et al. (2004). A PINOID-dependent binary switch in apical-basal PIN polar targeting directs auxin efflux. *Science* **306**, 862-865.

Geldner, N., Anders, N., Wolters, H., Keicher, J., Kornberger, W., Muller, P., Delbarre, A., Ueda, T., Nakano, A. and Jürgens, G. (2003). The Arabidopsis GNOM ARF-GEF mediates endosomal recycling, auxin transport, and auxin-dependent plant growth. *Cell* **112**, 219-230.

Grieneisen, V. A., Xu, J., Marée, A. F. M., Hogeweg, P. and Scheres, B. (2007). Auxin transport is sufficient to generate a maximum and gradient guiding root growth. *Nature* **449**, 1008-1013.

Grunewald, W. and Friml, J. (2010). The march of the PINs: developmental plasticity by dynamic polar targeting in plant cells. *EMBO J.* **29**, 2700-2714.

Habets, M. E. J. and Offringa, R. (2014). PIN-driven polar auxin transport in plant developmental plasticity: a key target for environmental and endogenous signals. *New Phytol.* **203**, 362-377.

Hammond, G. R. and Balla, T. (2015). Polyphosphoinositide binding domains: key to inositol lipid biology. *Biochim. Biophys. Acta* **1851**, 746-758.

Hammond, G. R., Fischer, M. J., Anderson, K. E., Holdich, J., Koteci, A., Balla, T. and Irvine, R. F. (2012). PI4P and PI(4,5)P2 are essential but independent lipid determinants of membrane identity. *Science* **337**, 727-730.

Hansson, M. D., Rzeznicka, K., Rosenback, M., Hansson, M. and Sirijovski, N. (2008). PCR-mediated deletion of plasmid DNA. *Anal. Biochem.* **375**, 373-375.

Heilmann, I. (2009). Using genetic tools to understand plant phosphoinositide signalling. *Trends Plant Sci.* **14**, 171-179.

Heilmann, I. (2016). Phosphoinositide signaling in plant development. *Development* **143**, 2044-2055.

Heilmann, M. and Heilmann, I. (2015). Plant phosphoinositides-complex networks controlling growth and adaptation. *Biochim. Biophys. Acta* **1851**, 759-769.

Heisler, M. G., Hamant, O., Krupinski, P., Uyttewaal, M., Ohno, C., Jönsson, H., Traas, J. and Meyerowitz, E. M. (2010). Alignment between PIN1 polarity and microtubule orientation in the shoot apical meristem reveals a tight coupling between morphogenesis and auxin transport. *PLoS Biol.* **8**, e1000516.

Helling, D., Possart, A., Cottier, S., Klahre, U. and Kost, B. (2006). Pollen tube tip growth depends on plasma membrane polarization mediated by tobacco PLC3 activity and endocytic membrane recycling. *Plant Cell* **18**, 3519-3534.

Heo, W. D., Inoue, T., Park, W. S., Kim, M. L., Park, B. O., Wandless, T. J. and Meyer, T. (2006). PI(3,4,5)P3 and PI(4,5)P2 lipids target proteins with polybasic clusters to the plasma membrane. *Science* **314**, 1458-1461.

Hirano, T., Munnik, T. and Sato, M. H. (2015). Phosphatidylinositol 3-phosphate 5-kinase, FAB1/PIKfyve kinase mediates endosome maturation to establish endosome-cortical microtubule interaction in Arabidopsis. *Plant Physiol.* **169**, 1961-1974.

Ischebeck, T., Seiler, S. and Heilmann, I. (2010). At the poles across kingdoms: phosphoinositides and polar tip growth. *Protoplasma* **240**, 13-31.

Ischebeck, T., Werner, S., Krishnamoorthy, P., Lerche, J., Meijon, M., Stenzel, I., Lofke, C., Wiessner, T., Im, Y. J., Perera, I. Y. et al. (2013). Phosphatidylinositol 4,5-bisphosphate influences PIN polarization by controlling clathrin-mediated membrane trafficking in Arabidopsis. *Plant Cell* **25**, 4894-4911.

Jaillais, Y., Fobis-Loisy, I., Miège, C., Rollin, C. and Gaude, T. (2006). AtSNX1 defines an endosome for auxin-carrier trafficking in Arabidopsis. *Nature* **443**, 106-109.

Jaillais, Y., Hothorn, M., Belkhadir, Y., Dabi, T., Nimchuk, Z. L., Meyerowitz, E. M. and Chory, J. (2011). Tyrosine phosphorylation controls brassinosteroid receptor activation by triggering membrane release of its kinase inhibitor. *Genes Dev.* **25**, 232-237.

Julkowska, M. M., Rankenberg, J. M. and Testerink, C. (2013). Liposome-binding assays to assess specificity and affinity of phospholipid-protein interactions. *Methods Mol. Biol.* **1009**, 261-271.

Katsiarimpa, A., Anzenberger, F., Schlager, N., Neubert, S., Hauser, M. T., Schwechheimer, C. and Isono, E. (2011). The Arabidopsis deubiquitinating enzyme AMSH3 interacts with ESCRT-III subunits and regulates their localization. *Plant Cell* **23**, 3026-3040.

Kleine-Vehn, J., Huang, F., Naramoto, S., Zhang, J., Michniewicz, M., Offringa, R. and Friml, J. (2009). PIN Auxin efflux carrier polarity is regulated by PINOID kinase-mediated recruitment into GNOM-independent trafficking in Arabidopsis. *Plant Cell* **21**, 3839-3849.

Kleine-Vehn, J. R., Ding, Z., Jones, A. R., Tasaka, M., Morita, M. T. and Friml, J. (2010). Gravity-induced PIN transcytosis for polarization of auxin fluxes in gravity-sensing root cells. *Proc. Natl. Acad. Sci. USA* **107**, 22344-22349.

Kleine-Vehn, J., Wabnik, K., Martiniere, A., Langowski, L., Willig, K., Naramoto, S., Leitner, J., Tanaka, H., Jakobs, S., Robert, S. et al. (2011). Recycling, clustering, and endocytosis jointly maintain PIN auxin carrier polarity at the plasma membrane. *Mol. Syst. Biol.* **7**, 540.

Kong, S.-G., Suzuki, T., Tamura, K., Mochizuki, N., Hara-Nishimura, I. and Nagatani, A. (2006). Blue light-induced association of phototropin 2 with the Golgi apparatus. *Plant J.* **45**, 994-1005.

Kusano, H., Testerink, C., Vermeer, J. E. M., Tsuge, T., Shimada, H., Oka, A., Munnik, T. and Aoyama, T. (2008). The Arabidopsis phosphatidylinositol phosphate 5-kinase PIP5K3 is a key regulator of root hair tip growth. *Plant Cell* **20**, 367-380.

Leyser, O. (2010). The power of auxin in plants. *Plant Physiol.* **154**, 501-505.

DEVELOPMENT

Li, G. and Xue, H.-W. (2007). Arabidopsis PLDzeta2 regulates vesicle trafficking and is required for auxin response. *Plant Cell* **19**, 281-295.

Li, L., Shi, X., Guo, X., Li, H. and Xu, C. (2014). Ionic protein-lipid interaction at the plasma membrane: what can the charge do? *Trends Biochem. Sci.* **39**, 130-140.

Lutz, U., Pose, D., Pfeifer, M., Gundlach, H., Hagmann, J., Wang, C., Weigel, D., Mayer, K. F., Schmid, M. and Schwechheimer, C. (2015). Modulation of ambient temperature-dependent flowering in Arabidopsis thaliana by natural variation of FLOWERING LOCUS M. *PLoS Genet.* **11**, e1005588.

Maures, T. J., Su, H.-W., Argetsinger, L. S., Grinstein, S. and Carter-Su, C. (2011). Phosphorylation controls a dual-function polybasic nuclear localization sequence in the adapter protein SH2B1β to regulate its cellular function and distribution. *J. Cell Sci.* **124**, 1542-1552.

McCaffrey, L. M. and Macara, I. G. (2009). Widely conserved signaling pathways in the establishment of cell polarity. *Cold Spring Harb. Perspect. Biol.* **1**, a001370.

McLaughlin, S. and Murray, D. (2005). Plasma membrane phosphoinositide organization by protein electrostatics. *Nature* **438**, 605-611.

Meijer, H. J. G. and Munnik, T. (2003). Phospholipid-based signaling in plants. *Annu. Rev. Plant Biol.* **54**, 265-306.

Michniewicz, M., Zago, M. K., Abas, L., Weijers, D., Schweighofer, A., Meskiene, I., Heisler, M. G., Ohno, C., Zhang, J., Huang, F. et al. (2007). Antagonistic regulation of PIN phosphorylation by PP2A and PINOID directs auxin flux. *Cell* **130**, 1044-1056.

Mironova, V. V., Omelyanchuk, N. A., Yosiphon, G., Fadeev, S. I., Kolchanov, N. A., Mjolsness, E. and Likhoshvai, V. A. (2010). A plausible mechanism for auxin patterning along the developing root. *BMC Syst. Biol.* **4**, 98.

Munnik, T. and Nielsen, E. (2011). Green light for polyphosphoinositide signals in plants. *Curr. Opin. Plant Biol.* **14**, 489-497.

Novakova, P., Hirsch, S., Feraru, E., Tejos, R., van Wijk, R., Viaene, T., Heilmann, M., Lerche, J., De Rycke, R., Feraru, M. I. et al. (2014). SAC phosphoinositide phosphatases at the tonoplast mediate vacuolar function in Arabidopsis. *Proc. Natl. Acad. Sci. USA* **111**, 2818-2823.

Offringa, R. and Huang, F. (2013). Phosphorylation-dependent trafficking of plasma membrane proteins in animal and plant cells. *J. Integr. Plant Biol.* **55**, 789-808.

Orlando, K. and Guo, W. (2009). Membrane organization and dynamics in cell polarity. *Cold Spring Harb. Perspect. Biol.* **1**, a001321.

Pan, X., Chen, J. and Yang, Z. (2015). Auxin regulation of cell polarity in plants. *Curr. Opin. Plant Biol.* **28**, 144-153.

Potocký, M., Pleskot, R., Pejchar, P., Vitale, N., Kost, B. and Žársky, V. (2014). Live-cell imaging of phosphatidic acid dynamics in pollen tubes visualized by Spo20p-derived biosensor. *New Phytol.* **203**, 483-494.

Rademacher, E. H. and Offringa, R. (2012). Evolutionary adaptations of plant AGC kinases: from light signaling to cell polarity regulation. *Front. Plant Sci.* **3**, 250.

Rakusová, H., Gallego-Bartolomé, J., Vanstraelen, M., Robert, H. S., Alabadí, D., Blázquez, M. A., Benková, E. and Friml, J. (2011). Polarization of PIN3-dependent auxin transport for hypocotyl gravitropic response in Arabidopsis thaliana. *Plant J.* **67**, 817-826.

Sachs, T. (1991). Cell polarity and tissue patterning in plants. *Development* **113**, 83-93.

Sakamoto, K. and Briggs, W. R. (2002). Cellular and subcellular localization of phototropin 1. *Plant Cell* **14**, 1723-1735.

Schindelin, J., Arganda-Carreras, I., Frise, E., Kaynig, V., Longair, M., Pietzsch, T., Preibisch, S., Rueden, C., Saalfeld, S., Schmid, B. et al. (2012). Fiji: an open-source platform for biological-image analysis. *Nat. Methods* **9**, 676-682.

Schmick, M., Vartak, N., Papke, B., Kovacevic, M., Truxius, D. C., Rossmannek, L. and Bastiaens, P. I. H. (2014). KRas localizes to the plasma membrane by spatial cycles of solubilization, trapping and vesicular transport. *Cell* **157**, 459-471.

Shewan, A., Eastburn, D. J. and Mostov, K. (2011). Phosphoinositides in cell architecture. *Cold Spring Harb. Perspect. Biol.* **3**, a004796.

Simon, M. L. A., Platre, M. P., Assil, S., van Wijk, R., Chen, W. Y., Chory, J., Dreux, M., Munnik, T. and Jaillais, Y. (2014). A multi-colour/multi-affinity marker set to visualize phosphoinositide dynamics in Arabidopsis. *Plant J.* **77**, 322-337.

Simon, M. L. A., Platre, M. P., Marquès-Bueno, M. M., Armengot, L., Stanislas, T., Bayle, V., Caillaud, M.-C. and Jaillais, Y. (2016). A PtdIns(4)P-driven electrostatic field controls cell membrane identity and signalling in plants. *Nat. Plants* **2**, 16089.

Stahelin, R. V., Scott, J. L. and Frick, C. T. (2014). Cellular and molecular interactions of phosphoinositides and peripheral proteins. *Chem. Phys. Lipids* **182**, 3-18.

Stanislas, T., Hüser, A., Barbosa, I. C. R., Kiefer, C. S., Brackmann, K., Pietra, S., Gustavsson, A., Zourelidou, M., Schwechheimer, C. and Grebe, M. (2015). D6 PROTEIN KINASE is a lipid domain-dependent mediator of Arabidopsis planar polarity. *Nat. Plants* **1**, 15162.

Stenzel, I., Ischebeck, T., Konig, S., Holubowska, A., Sporysz, M., Hause, B. and Heilmann, I. (2008). The type B phosphatidylinositol-4-phosphate 5-kinase 3 is essential for root hair formation in Arabidopsis thaliana. *Plant Cell* **20**, 124-141.

Teale, W. D., Paponov, I. A. and Palme, K. (2006). Auxin in action: signalling, transport and the control of plant growth and development. *Nat. Rev. Mol. Cell Biol.* **7**, 847-859.

Tejos, R., Sauer, M., Vanneste, S., Palacios-Gomez, M., Li, H., Heilmann, M., van Wijk, R., Vermeer, J. E. M., Heilmann, I., Munnik, T. et al. (2014). Bipolar plasma membrane distribution of phosphoinositides and their requirement for auxin-mediated cell polarity and patterning in Arabidopsis. *Plant Cell* **26**, 2114-2128.

van Berkel, K., de Boer, R. J., Scheres, B. and ten Tusscher, K. (2013). Polar auxin transport: models and mechanisms. *Development* **140**, 2253-2268.

Vermeer, J. E. M., van Leeuwen, W., Tobeña-Santamaria, R., Laxalt, A. M., Jones, D. R., Divecha, N., Gadella, T. W., Jr. and Munnik, T. (2006). Visualization of PtdIns3P dynamics in living plant cells. *Plant J.* **47**, 687-700.

Vermeer, J. E. M., Thole, J. M., Goedhart, J., Nielsen, E., Munnik, T. and Gadella, T. W. J., Jr (2009). Imaging phosphatidylinositol 4-phosphate dynamics in living plant cells. *Plant J.* **57**, 356-372.

Vlahos, C. J., Matter, W. F., Hui, K. Y. and Brown, R. F. (1994). A specific inhibitor of phosphatidylinositol 3-kinase, 2-(4-morpholinyl)-8-phenyl-4H-1-benzopyran-4-one (LY294002). *J. Biol. Chem.* **269**, 5241-5248.

Wabnik, K., Govaerts, W., Friml, J. and Kleine-Vehn, J. (2011). Feedback models for polarized auxin transport: an emerging trend. *Mol. BioSys.* **7**, 2352-2359.

Wang, R. and Estelle, M. (2014). Diversity and specificity: auxin perception and signaling through the TIR1/AFB pathway. *Curr. Opin. Plant Biol.* **21C**, 51-58.

Willige, B. C., Ahlers, S., Zourelidou, M., Barbosa, I. C. R., Demarsy, E., Trevisan, M., Davis, P. A., Roelfsema, M. R. G., Hangarter, R., Fankhauser, C. et al. (2013). D6PK AGCVIII kinases are required for auxin transport and phototropic hypocotyl bending in Arabidopsis. *Plant Cell* **25**, 1674-1688.

Yang, Z. (2008). Cell polarity signaling in Arabidopsis. *Annu. Rev. Cell Dev. Biol.* **24**, 551-575.

Yeung, T., Gilbert, G. E., Shi, J., Silvius, J., Kapus, A. and Grinstein, S. (2008). Membrane phosphatidylserine regulates surface charge and protein localization. *Science* **319**, 210-213.

Zegzouti, H., Li, W., Lorenz, T. C., Xie, M., Payne, C. T., Smith, K., Glenny, S., Payne, G. S. and Christensen, S. K. (2006). Structural and functional insights into the regulation of Arabidopsis AGC VIIIa kinases. *J. Biol. Chem.* **281**, 35520-35530.

Zhao, Y., Yan, A., Feijó, J. A., Furutani, M., Takenawa, T., Hwang, I., Fu, Y. and Yang, Z. (2010). Phosphoinositides regulate clathrin-dependent endocytosis at the tip of pollen tubes in Arabidopsis and tobacco. *Plant Cell* **22**, 4031-4044.

Zourelidou, M., Müller, I., Willige, B. C., Nill, C., Jikumaru, Y., Li, H. and Schwechheimer, C. (2009). The polarly localized D6 PROTEIN KINASE is required for efficient auxin transport in Arabidopsis thaliana. *Development* **136**, 627-636.

Zourelidou, M., Absmanner, B., Weller, B., Barbosa, I. C. R., Willige, B. C., Fastner, A., Streit, V., Port, S., Colcombet, J., van Bentem, S. et al. (2014). Auxin efflux by PIN-FORMED proteins is activated by two different protein kinases, D6 PROTEIN KINASE and PINOID. *Elife* **3**, e02860.

DEVELOPMENT